© 2021. Published by The Company of Biologists Ltd | Journal of Cell Science (2021) 134, jcs248237. doi:10.1242/jcs.248237

RESEARCH ARTICLE

The tight junction protein Claudin-5 limits endothelial cell motility

Zhenguo Yang[1,*], Shuilong Wu[1,*], Federica Fontana[2,*], Yanyu Li[1], Wei Xiao[1], Zhangdai Gao[1], Alice Krudewig[3], Markus Affolter[3], Heinz-Georg Belting[3], Salim Abdelilah-Seyfried[2,4,‡] and Jingjing Zhang[1,‡]

ABSTRACT

Steinberg's differential adhesion hypothesis suggests that adhesive mechanisms are important for sorting of cells and tissues during morphogenesis (Steinberg, 2007). During zebrafish vasculogenesis, endothelial cells sort into arterial and venous vessel beds but it is unknown whether this involves adhesive mechanisms. Claudins are tight junction proteins regulating the permeability of epithelial and endothelial tissue barriers. Previously, the roles of claudins during organ development have exclusively been related to their canonical functions in determining paracellular permeability. Here, we use atomic force microscopy to quantify claudin-5-dependent adhesion and find that this strongly contributes to the adhesive forces between arterial endothelial cells. Based on genetic manipulations, we reveal a non-canonical role of Claudin-5a during zebrafish vasculogenesis, which involves the regulation of adhesive forces between adjacent dorsal aortic endothelial cells. *In vitro* and *in vivo* studies demonstrate that loss of claudin-5 results in increased motility of dorsal aorta endothelial cells and in a failure of the dorsal aorta to lumenize. Our findings uncover a novel role of claudin-5 in limiting arterial endothelial cell motility, which goes beyond its traditional sealing function during embryonic development.

KEY WORDS: Claudin-5, Adhesive force, Dorsal aorta, Atomic force microscopy, Vasculogenesis, Cell motility

INTRODUCTION

The formation of a vascular network is an essential process during early embryogenesis. This involves the migration of arterial and venous angioblasts (endothelial progenitor cells) to the embryonic midline, where they assemble into vessel beds, establish cell junctions, rearrange into tubular structures and generate a lumenized network of blood vessels (Jin et al., 2005; Strilić et al., 2010; Yu et al., 2015). Subsequently, endothelial cells (ECs) that form the inner linings of arteries and veins adapt to their different physiological roles within the cardiovascular network by acquiring morphological and molecular differences. For instance, arterial ECs establish tight junction (TJ)-based barrier systems, which seal blood vessels against the paracellular movement of water, whereas venous ECs form less-dense TJs that are more leaky (Schneeberger, 1982).

The barrier properties of many tissues are dependent on claudins, a family of four-transmembrane TJ proteins (Kollmar et al., 2001; Krause et al., 2008; Lal-Nag and Morin, 2009; Loh et al., 2004). These proteins have also been shown to possess adhesive properties (Kubota et al., 1999). Functional studies in mouse revealed an important role of claudin-5 (Cldn5) in controlling the permeability of the cerebrovascular blood–brain barrier (Nitta et al., 2003). In zebrafish, Cldn5a has an essential function in the tightening of a neuroepithelial barrier during hydrostatic pressure-driven brain ventricle expansion (Zhang et al., 2010), but its potential developmental roles within the vasculature have not yet been characterized (Fleming et al., 2013; Jin et al., 2005; Xie et al., 2010).

Besides the canonical roles of claudins on the regulation of the physiological barrier functions, recent studies have also revealed an involvement of claudins in tumor progression which included affecting the migration, invasion and metastasis of cancer cells (Ma et al., 2017). For instance, during carcinogenesis of colorectal cancer, the changes of cell interactions and tissue morphology are accompanied by expression changes of various claudin genes (Bujko et al., 2015). In breast cancer, rather than tightening the cell barrier, Cldn5 affects the cell motility through the N-WASP and ROCK signaling pathways (Escudero-Esparza et al., 2012). One way claudins may change endothelial or epithelial cell motility is by impacting cell adhesion.

In zebrafish, two *cldn5* paralogs (*cldn5a* and *cldn5b*) are expressed during embryonic developmental stages (van Leeuwen et al., 2018; Zhang et al., 2010). Cldn5a has a neuroepithelial and dorsal aorta expression, while Cldn5b is restricted to the arterial vessel system including the dorsal aorta (Zhang et al., 2010). We previously showed that Cldn5a has an essential sealing function in a neuroepithelial barrier during hydrostatic pressure-driven brain ventricle expansion (Zhang et al., 2010). In contrast, whether Cldn5 proteins have developmental roles in the zebrafish vasculature has not yet been determined. During zebrafish embryonic vasculogenesis, Cldn5 proteins are first detectable at 18 h post fertilization (hpf) in arterial endothelial cells marking endothelial cell–cell junctions of the trunk region (Jin et al., 2005). In the zebrafish brain, *cldn5a* is expressed in the cerebrovasculature after 48 hpf, while *cldn5b* is expressed within cerebral vascular endothelial cells as early as 30 hpf (Zhang, 2010). Functional studies revealed that the zebrafish blood–brain barrier matures after 2 days post fertilization (dpf) (Fleming et al., 2013; Jeong et al., 2008; van Leeuwen et al., 2018; Xie et al., 2010). However, previous studies did not address whether endothelial Cldn5 proteins may have developmental roles during vasculogenesis before 48 hpf.

In this study, we quantify the important contribution of Cldn5 to EC adhesive forces and motility. We also address the role of Cldn5a in the nascent zebrafish dorsal aorta and find that it limits EC motility during vasculogenesis and is required for the lumenization of the dorsal aorta.

[1]Affiliated Hospital of Guangdong Medical University & Key Laboratory of Zebrafish Model for Development and Disease, Guangdong Medical University, Zhanjiang 524001, China. [2]Institute of Biochemistry and Biology, Potsdam University, D-14476 Potsdam, Germany. [3]Department of Cell Biology, Biozentrum der Universität Basel, Klingelbergstrasse 70, CH-4056 Basel, Switzerland. [4]Institute of Molecular Biology, Hannover Medical School, Carl-Neuberg Str. 1, D-30625 Hannover, Germany.
*These authors contributed equally to this work

‡Authors for correspondence (jingjing.zhang@live.com; salim.seyfried@uni-potsdam.de)

Z.Y., 0000-0002-7768-1508; S.W., 0000-0001-9589-1405; W.X., 0000-0003-1815-7391; Z.G., 0000-0002-8986-7932; H.-G.B., 0000-0002-1538-4364; J.Z., 0000-0002-8789-4638

Handling Editor: Kathleen Green
Received 29 April 2020; Accepted 26 November 2020

Journal of Cell Science (2021) 134, jcs248237. doi:10.1242/jcs.248237

RESULTS

Cldn5 reduces EC motility

The TJ protein Cldn5 has a well-characterized role in controlling the permeability properties of endothelial tissues and of the blood–brain barrier (Chen et al., 2017b; Nitta et al., 2003). To investigate to what extent Cldn5 impacts EC motility, we applied *in vitro* analyses based on the knockdown of *Cldn5* in murine brain microvascular ECs (bEnd.3 cells). We reasoned that a reduction of Cld5 may result in a quantifiable increase in cell motility. When transfecting these ECs with mouse-specific *Cldn5* short hairpin RNA (*shCldn5*-bEnd.3), Cldn5 protein expression was efficiently blocked in comparison with control vector-transfected cells (*shCtrl*-bEnd.3) (Fig. 1A). The expression of the TJ-associated protein ZO-1 (also known as TJP1) was not affected by this knockdown approach (Fig. 1A). Subsequently, we used these cells for a well-established trans-well membrane migration assay (Justus et al., 2014). When control bEnd.3 or *shCldn5*-bEnd.3 cells were incubated in trans-well insets for 24 h, *shCldn5*-bEnd.3 cells exhibited a significantly higher degree of motility and migrated through the trans-well membrane towards the bottom more efficiently than control bEnd.3 cells. This migration behavior was assayed using a Crystal Violet staining protocol that clearly marks ECs. It allowed us to quantify the proportion from total of ECs that migrated to the outside membrane of the well (Fig. 1B,C). We also observed an enhanced motility of *shCldn5*-bEnd.3 cells compared with control bEnd.3 cells when EC migration was further stimulated by adding endothelial cell growth factor (ECGF) to the

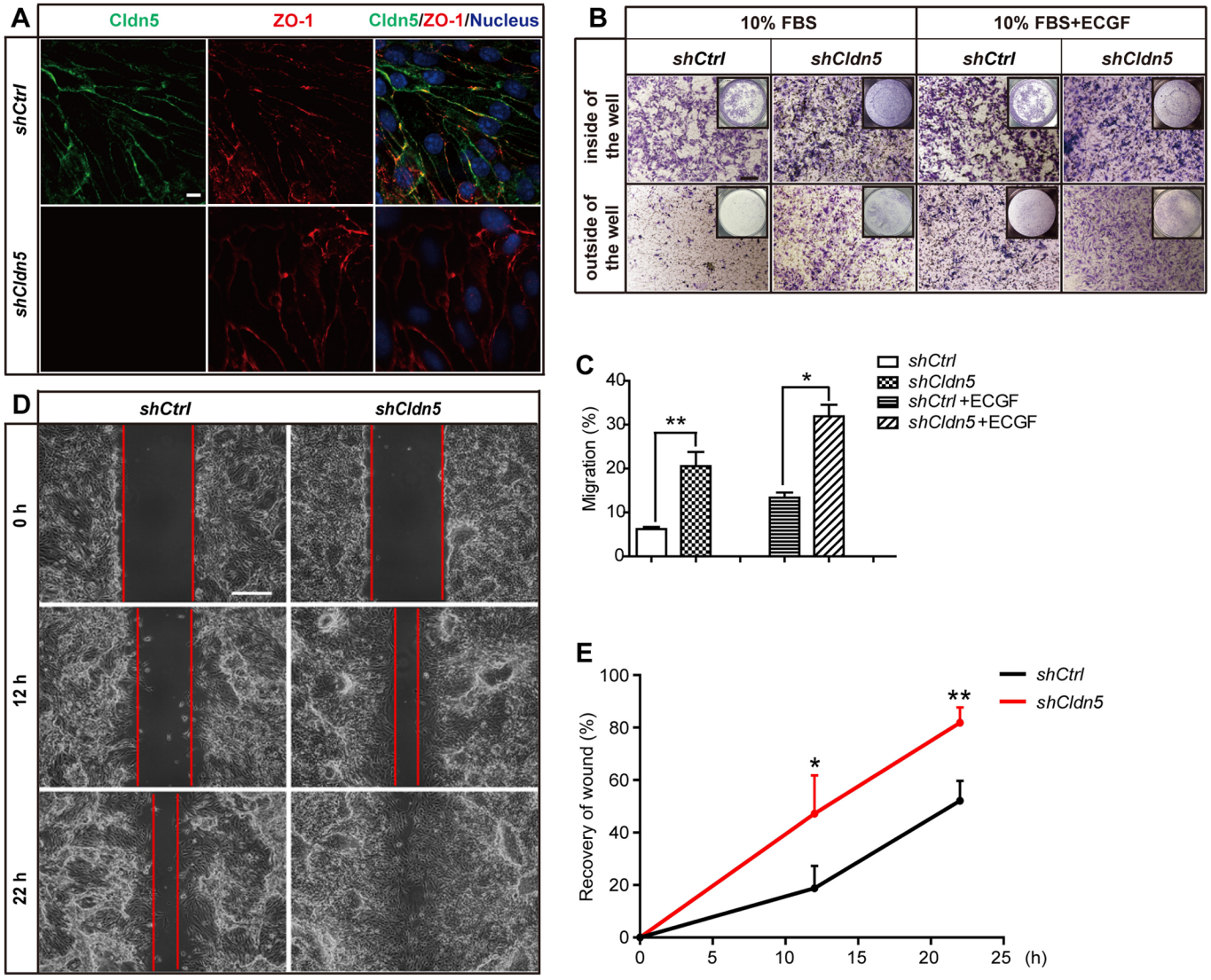

Fig. 1. shRNA-mediated knockdown of *Cldn5* in bEnd.3 cells increases cell motility. (A) *Cldn5* is efficiently knocked down by short hairpin RNA (*shCldn5*) as shown by anti-Cldn5 immunolabeling, which overlaps with anti-ZO-1 staining. (B) Cell migration assay for quantifying the migration rate of endothelial cells from inside the well (24-well format, with 8 µm pore size inserts) through a transwell membrane to the outside. Shown are Crystal Violet-stained cells on both inside and outside of the transwell membrane. Insets are the images of the whole membrane after cell staining. In comparison with control vector-transfected bEnd.3 cells (*shCtrl*), loss of Cldn5 (*shCldn5*) increases cell motility under conditions with or without stimulation by endothelial cell growth factor (ECGF). (C) Quantifications of cell motility assays, representing the mean±s.e.m. percentage of cells that migrated to the outside membrane of the well. (D) Representative images of wound healing assays with *shCtrl* or *shCldn5* bEnd.3 cells. Images were taken at 0, 12 and 24 h respectively after the cell layer was scratched with a pipette tip. (E) Statistical analyses (mean±s.e.m.) of the recovery rate of the wound indicated a significantly increased migration ability of bEnd.3 cells after loss of Cldn5 compared with that of the control group. n=3 tests per group. *P<0.05, **P<0.01 (unpaired two-tailed Student's t-test). Scale bars: 10 µm (A); 100 µm (B); 250 µm (D).

Journal of Cell Science (2021) 134, jcs248237. doi:10.1242/jcs.248237

bottom well (Fig. 1B,C). To further support this finding, a classic wound healing assay was performed with *shCtrl*-bEnd.3 and *shCldn5*-bEnd.3 cells. After 10 or 22 h of culturing, *shCldn5*-bEnd.3 cells had recovered more strongly compared with control bEnd.3 cells (Fig. 1D,E). This finding indicates that bEnd.3 cells have an increased migration ability upon loss of Cldn5. To confirm these results, we also generated stabilized bEnd.3 *Cldn5*$^{-/-}$ lines by CRISPR/Cas9-mediated knockout of Cldn5 in bEnd.3 cells (Fig. S1A,B). The wound healing experiment revealed that within 22 h of culturing, bEnd.3 *Cldn5*$^{-/-}$ cells had more strongly recovered and showed higher rate of motility compared with the wild-type bEnd.3 cells (Fig. S1C). Meanwhile, we performed a CRISPR/Cas9-mediated knockout of Cldn5 in another endothelial line, human brain microvascular ECs (HBMECs), which under wild-type conditions express high levels of Cldn5 (Fig. S2A,B). Within 12 h of culturing, HBMEC *Cldn5*$^{-/-}$ cells showed a higher rate of motility and covered the wound area faster than the control HBMEC cells (Fig. S2C). These results suggest that the expression of Cldn5 has a limiting effect on EC motility.

Claudin-5 is required for EC adhesion

Claudins are transmembrane proteins, and can interact with other claudins through homo- or hetero-philic *trans*-interactions between neighboring cells. Cldn5 seals the paracellular space by interacting, via face-to-face homophilic *trans*-interactions, between neighboring cells during the formation of TJ strands (Piorntek et al., 2008). Our findings showing that Cldn5 limits the motility of murine ECs in a transwell membrane migration assay, suggest that it might play a role in cell adhesion that goes beyond its well-established function in tight junctional sealing. To measure the strength of Cldn5-dependent adhesive forces between ECs, we performed a bead-rolling assay (Strilić et al., 2010). This assay measures the ability of EC-covered beads to roll down a slightly tilted EC monolayer-coated plate in a gravity-driven manner. Hence, the rolling distance covered by the beads inversely correlates with the adhesive strength of cell–cell contacts (Strilić et al., 2010). After incubation of ECs on collagen-coated glass beads, we found that Cldn5 was depleted from *shCldn5*-bEnd.3 ECs (Fig. 2A,B). In the bead-rolling-assay (Fig. 2C), beads coated with *shCldn5*-bEnd.3 ECs covered a significantly longer rolling distance on either *shCtrl*-bEnd.3 EC- or *shCldn5*-bEnd.3 EC-coated tilting plates, compared to a setup in which both beads and tilting plate were coated with the control-silenced *shCtrl*-bEnd.3 ECs (Fig. 2D,E). Similarly, beads coated with control-silenced ECs rolled a significantly longer distance when placed on tilting plates coated with Cldn5-depleted ECs compared with the distance covered over tilting plates coated with control-silenced ECs or over basal control tilting plates (Fig. 2D,E; Movies 1–4). Similar results were observed from the bead-rolling analyses with stabilized *Cldn5*-knockout bEnd.3 cells, where beads coated with bEnd.3 *Cldn5*$^{-/-}$ cells covered a significantly longer rolling distance on both wild-type bEnd.3 EC- and bEnd.3 *Cldn5*$^{-/-}$ EC-coated tilting plates, compared to a setup in which both beads and tilting plate were coated with the wild-type bEnd.3 ECs (Fig. S1D). These results demonstrate that Cldn5 generates cell–cell adhesion forces between adjacent ECs.

To quantify the strengths of adhesive forces between ECs, we also used atomic force microscopy (AFM) (Puech et al., 2005). We cultured control bEnd.3 ECs for at least 3 days on glass beads until they expressed Cldn5 (Fig. 2A,B) prior to fixing these beads onto the AFM cantilever (Fig. 2F). Next, the AFM cantilever holding bEnd.3 cell-coated beads was allowed to attach to the basal substratum with cultured ECs for at least 5 min to ensure a full face-to-face contact. Using AFM, we recorded the force needed to separate EC-coated beads from contacting with basal ECs on a disc. These measurements revealed adhesive forces of 1245.04±280.18 pN (means±s.d.) between Cldn5-expressing control ECs, while adhesion forces were only 423.36±212.41 pN between Cldn5-deficient *shCldn5*-bEnd.3 ECs, 453.78±83.14 pN between Cldn5-deficient ECs and control ECs, and 381.38±97.29 pN between control ECs and Cldn5-deficient ECs (Fig. 2G). Taken together, these measurements demonstrate that Cldn5 strongly affects EC adhesion.

Claudin-5a limits endothelial cell motility and promotes lumenization during vasculogenesis of the dorsal aorta in zebrafish

The above findings suggest that Cldn5 may play some developmental role by affecting EC adhesion and motility. The zebrafish genome contains two genes encoding paralogs of mammalian Cldn5, Cldn5a [zgc:85723] and Cldn5b [zgc:103419], of which Cldn5a is more similar to mammalian Cldn5 (van Leeuwen et al., 2018; Zhang et al., 2012; Zhang et al., 2010). To elucidate the precise pattern of gene expressions of zebrafish *cldn5a* and *cldn5b* during early embryonic vascular development, we performed whole-mount *in situ* hybridizations (WISH) on 30 hpf zebrafish embryos. Consistent with previous reports, *cldn5a* was expressed within the zebrafish dorsal aorta and in neuroepithelial cells of the brain and spinal cord (Fig. 3A) (van Leeuwen et al., 2018; Zhang et al., 2010). In comparison, *cldn5b* was expressed in a partially overlapping pattern in arterial ECs, including the dorsal aorta but not the caudal vein (Fig. 3B).

To characterize developmental roles of *cldn5a* and *cldn5b* within the vasculature, we generated loss-of-function mutants using CRISPR/Cas9 genome-editing strategies. This approach yielded two *cldn5a* loss-of-function alleles (*cldn5a*$^{\Delta 8}$ with an 8 bp deletion and *cldn5a*$^{\Delta 14}$ with a 14 bp deletion) encoding predicted truncations of Cldn5a at the second transmembrane domain (Fig. 3C). This approach also resulted in a *cldn5b* loss of function allele (*cldn5b*$^{\Delta 130}$ with a 130 bp deletion) causing a similar predicted truncation at the second transmembrane domain (Fig. 3D).

Since both *cldn5* paralogous genes were co-expressed within the dorsal aorta, we first characterized the morphology of this blood vessel in *cldn5b* and *cldn5a* single mutants and also in *cldn5a*$^{\Delta 14/\Delta 14}$; *cldn5b*$^{\Delta 130/\Delta 130}$ double mutants. We found that *cldn5b*$^{\Delta 130/\Delta 130}$ single mutants did not show any obvious phenotype compared with wild-type (Fig. 3E,F,K). Strikingly, in *cldn5a*$^{\Delta 14/\Delta 14}$ single mutants and *cldn5a*$^{\Delta 14/\Delta 14}$;*cldn5b*$^{\Delta 130/\Delta 130}$ double mutants, the dorsal aorta failed to lumenize by 30 hpf (Fig. 3G–I,K). Consequently, the blood vessel diameter was massively reduced from 35.00±3.79 µm (means±s.d.) in wild type (Fig. 3E; *n*=5 embryos) to 11.40±1.02 µm in *cldn5a*$^{\Delta 14/\Delta 14}$ mutants (Fig. 3G; *n*=5 embryos), 9.00±1.26 µm in *cldn5a*$^{\Delta 8/\Delta 8}$ mutants (Fig. 3J; *n*=5 embryos) and 10.80±4.17 µm in *cldn5a*$^{\Delta 14/\Delta 14}$;*cldn5b*$^{\Delta 130/\Delta 130}$ double mutants (Fig. 3H; *n*=5 embryos). Immunohistochemical stainings using an anti-pan-Cldn5 antibody on tissue cross sections of embryos revealed that Cldn5 immunoreactivity, which was present in the dorsal aorta of wild-type embryos (Fig. 3E′), was entirely absent only in *cldn5a*$^{\Delta 14/\Delta 14}$; *cldn5b*$^{\Delta 130/\Delta 130}$ double mutants rather than in the individual mutants (Fig. 3F′–H′). Hence, both Cldn5 proteins have a partially overlapping expression within the dorsal aorta.

A similar failure of dorsal aorta lumen expansion was observed after antisense morpholino oligonucleotide (MO)-mediated knockdown of *cldn5a* (Zhang et al., 2010; Fig. S3A,C; Fig. 3L) and of *cldn5a* together with *cldn5b* (Fig. S3A,D; Fig. 3L), but not of *cldn5b* alone (Zhang, 2010; Fig. S3A,B; Fig. 3L). The diameter of the dorsal aorta lumen diminished from 39.80±4.40 µm in wild-type

Journal of Cell Science (2021) 134, jcs248237. doi:10.1242/jcs.248237

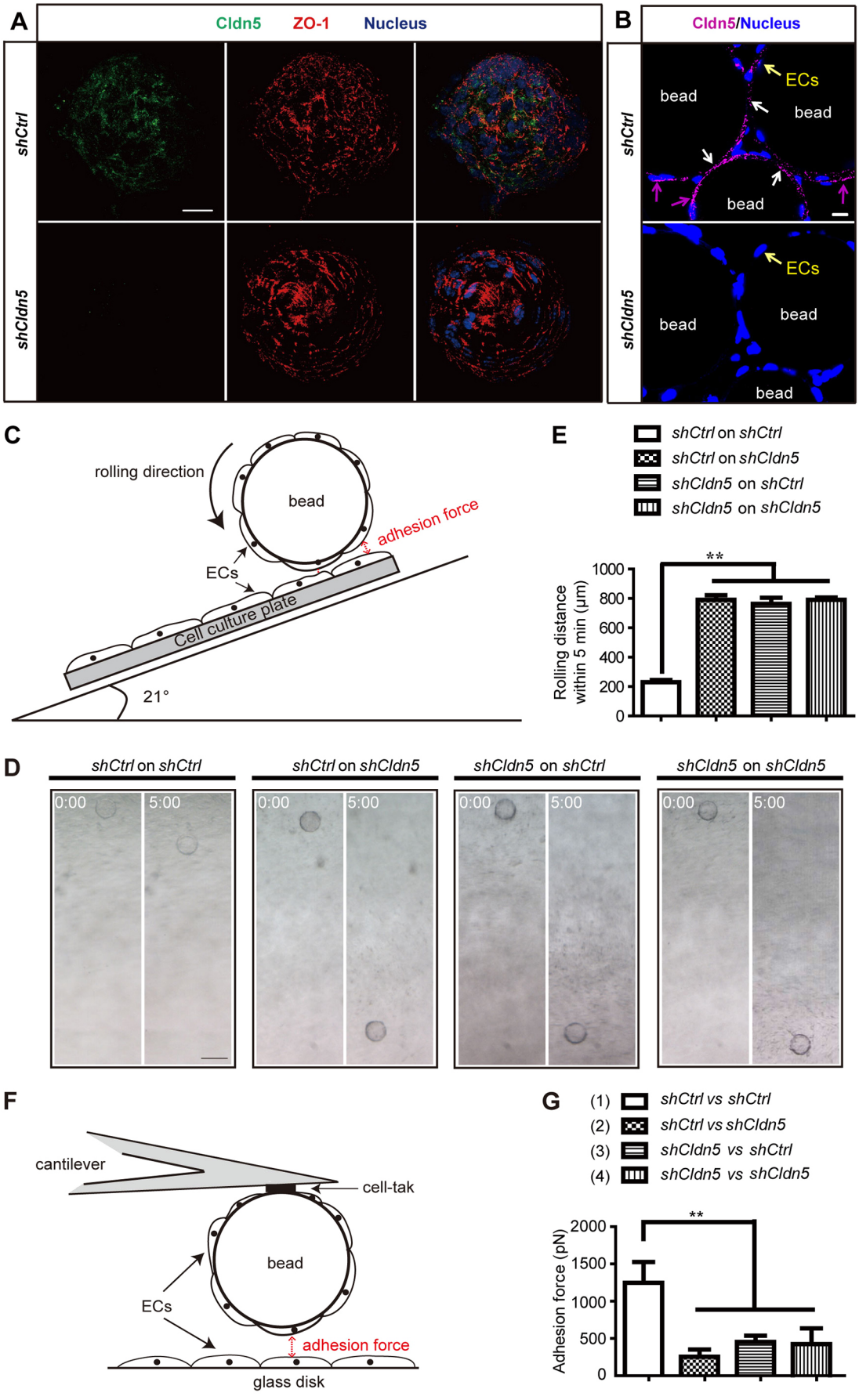

Fig. 2. See next page for legend.

Fig. 2. Assays for measuring Cldn5-dependent adhesion forces between endothelial cells. (A) Shown are confocal images of immunohistochemical stainings of EC-coated beads used for the 'rolling bead' assay. Endothelial bEnd.3 cells transfected either with a control vector (*shCtrl*) or with a vector for *Cldn5* knockdown (*shCldn5*) were seeded and cultured on glass beads. Immunolabeling of tight junction proteins ZO-1 and Cldn5 show that both proteins are expressed in *shCtrl* bEnd.3 cells grown on coated beads, whereas Cldn5 is depleted from *shCldn5*-transfected bEnd.3 cells. (B) After incubation of bEnd.3 cells on the surface of beads, Cldn5 is not only expressed on the cell–cell junctional surface of bEnd.3 cells from two contacting beads (white arrows), but is also detected on the apical surface and cell substratum of endothelial cells (purple arrows). (C) Schematic diagram of rolling bead assay for testing adhesion forces between bEnd.3 cells. Glass beads coated with bEnd.3 cells are placed onto a tilted (inclination of 21°) cell culture plate that is coated with a monolayer of *shCtrl*- or *shCldn5*-transfected bEnd.3 cells. For this assay, the rolling distance within 5 min correlates with the adhesive forces that act in *trans* between bEnd.3 cells on both sides (double sided red arrow). (D) Representative bright-field images (taken from Movies 1–4) showing EC-coated beads rolling on a tilted EC monolayer. Time is indicated in min:s. (E) Quantification (means±s.d.) of the rolling bead assay. Knockdown of *Cldn5* in bEnd.3 cells on either the culture plate or on the rolling bead reduces adhesion forces between endothelial cells. This correlates with a longer rolling distance in conditions with Cldn5-deficient bEnd.3 cells compared with that of *shCtrl* bEnd.3-coated beads on *shCtrl* bEnd.3-coated culture plates. n=5 tests per group. (F) Schematic diagram of adhesion force measurement between ECs based on atomic force microscope (AFM)-based single EC force spectroscopy (SCFS). This assay determines the physical strength of adhesion forces (in pN) between ECs coating the glass bead in *trans* with others covering the glass disk. Using this setup, four different *trans* conditions were measured: (1) control ECs on the beads and control ECs on the plate, (2) control ECs on the beads and Cldn5-deficient ECs on the plate, (3) Cldn5-deficient ECs on the beads and control ECs on the plate, and (4) Cldn5-deficient ECs on the beads and Cldn5-deficient cells on the plate. (G) Quantification (means±s.d.) of adhesion forces demonstrate that Cldn5-expressing *shCtrl* bEnd.3 cells establish stronger adhesion forces in trans compared with conditions in which at least one group of bEnd.3 cells is depleted of Cldn5 (either on the glass bead and/or on the glass plate). n=9 tests per group. These experiments suggest that Cldn5 acts via *trans*-interactions between endothelial cells to reduce EC motility. $^{**}P<0.01$ (unpaired two-tailed Student's t-test). Scale bars: 25 µm (A); 40 µm (B); 100 µm (D).

(n=5 embryos) to 5.20±2.98 µm in *cldn5a* morphants (n=5 embryos) and 9.40±4.72 µm in *cldn5a/b* double morphants (n=5 embryos). To verify the specificity of *cldn5a* MO, we co-injected exogenous *cldn5a* mRNA together with *cldn5a* MO, which significantly reduced the proportion of embryos with a defective dorsal aorta lumen expansion (Fig. 3L). When performing immunohistochemical stainings, the MO-based gene knockdown of both *cldn5a* and *cldn5b* entirely depleted Cldn5 protein from the dorsa aorta (Fig. S3D′,D″).

Morphological inspections also showed that the loss of Cldn5a or of Cldn5a/b caused vascular changes that went beyond mere lumen expansion defects. Vibratome cross sections of the trunk region revealed that the dorsal aorta and caudal vein were in tight contact in *cldn5a*$^{\Delta 14/\Delta 14}$ single mutants and *cldn5a*$^{\Delta 14/\Delta 14}$;*cldn5b*$^{\Delta 130/\Delta 130}$ double mutants (Fig. 3G″,H″), whereas these two vessels were clearly separated in wild-type (Fig. 3E″) and in *cldn5b*$^{\Delta 130/\Delta 130}$ single mutants (Fig. 3F″). Similarly, in *cldn5a* single morphants or *cldn5a/b* double morphants, some regions along the dorsal aorta were in close proximity with the posterior caudal vein, which is suggestive of a failure of these two vessel types to separate (Fig. S3C″,D″).

To complement the other knockout and knockdown approaches, we also used a novel CRISPR/Cas13a-mediated gene knockdown strategy (Abudayyeh et al., 2017; Gootenberg et al., 2017; Liu et al., 2017) for *cldn5a*. In *cldn5a* crispants, the diameter of the embryonic dorsal aorta was reduced to 14.82±5.00 µm at 30 hpf (n=4 embryos), which was significantly smaller than that of the only *cldn5a* crRNA-injected control embryos (32.85±3.69 µm, n=4 embryos) (Fig. S4A,B). To verify the efficacy of this method, we performed quantitative reverse transcription-PCR (qRT-PCR) of *cldn5a* mRNA levels, which were significantly reduced in *cldn5a* crispants (Fig. S4C). These findings suggest that Cldn5a plays a role in the separation of the dorsal aorta from venous ECs and in the lumen expansion of the dorsal aorta.

Claudin-5a limits motility of arterial endothelial cells during formation of the dorsal aorta

Because the expression of Cldn5 had a limiting effect on murine EC motility in *in vitro* assays, we wondered whether a loss of Cldn5a had an equal impact on the motility of dorsal aorta ECs during vasculogenesis. To address this question, we traced the migration of arterial ECs during early vasculogenesis between 17 and 24 hpf. Time-lapse imaging in the endothelial-specific transgenic reporter line *Tg(fli1a:nEGFP)*^{y7} combined with single-cell track analyses revealed that the motility of arterial ECs significantly increased with 5.35±0.33 µm/30 min (means±s.d.) in *cldn5a* morphants compared with 4.29±0.25 µm/30 min in wild-type embryos (Fig. 4A,B; Movies 5,6). Notably, the direction of ECs was primarily along the antero-posterior body axis in *cldn5a* morphants, whereas wild-type ECs had prominent trajectories in the dorsal-to-ventral direction (Fig. 4A,B). These data indicate that loss of Cldn5a causes a failure of morphogenesis due to reduced adhesion and increased motility of dorsal aorta ECs.

Expression of the EC adhesion factors PECAM-1 and integrin-β1, but not of VE-Cadherin, is dependent on Claudin-5a

Adhesive mechanisms play important roles during various morphogenetic processes (Kim et al., 2017; Yi et al., 2008). Molecular studies have shown that expression of cadherin is important for the control of cell adhesion and motility during development (De Pascalis and Etienne-Manneville, 2017). A loss of claudins in Madin–Darby canine kidney (MDCK) cells revealed alterations in the actomyosin cytoskeleton. This may impact cadherin-mediated cell adhesion (Otani et al., 2019). To assess whether the loss of Cldn5 affected the expression of *ve-cadherin*, we first performed WISH in *cldn5a* morphant zebrafish. We found that *ve-cadherin* mRNA expression was not affected upon loss of Cldn5a at 20–22 hpf (Fig. 5A). We also performed immunofluorescence imaging on vibratome cross sections through the zebrafish trunk region and found that loss of Cldn5a had no effect on the expression and localization of VE-Cadherin in aortic ECs (Fig. 5B). Similarly, VE-Cadherin was not reduced in both *shCtrl*-bEnd.3- or *shCldn5*-bEnd.3-ECs (Fig. 5C). Hence, the increase in EC motility in *cldn5* morphants is not related to a reduced expression of VE-Cadherin.

PECAM1 and integrin-β1 are typical endothelial adhesive molecules that may affect EC motility. Next, we investigated whether their expression was altered upon loss of Cldn5 in ECs. Based on immunohistochemical stainings, we found that the expression of PECAM-1 and integrin-β1 was reduced upon loss of Cldn5 (Fig. 5D,E), while levels of filamentous actin (F-actin), an essential cytoskeletal protein, were not altered in *shCldn5*-bEnd.3 cells when compared with *shCtrl*-bEnd.3 cells (Fig. 5F).

DISCUSSION

Our findings based on AFM measurements demonstrate that Cldn5 limits motility of murine ECs and that this may be important also within the nascent dorsal aorta of zebrafish. Unlike VE-cadherin, which is expressed ubiquitously within the vasculature, Cldn5 proteins are restricted to arterial vessel beds and play an important role in

Journal of Cell Science (2021) 134, jcs248237. doi:10.1242/jcs.248237

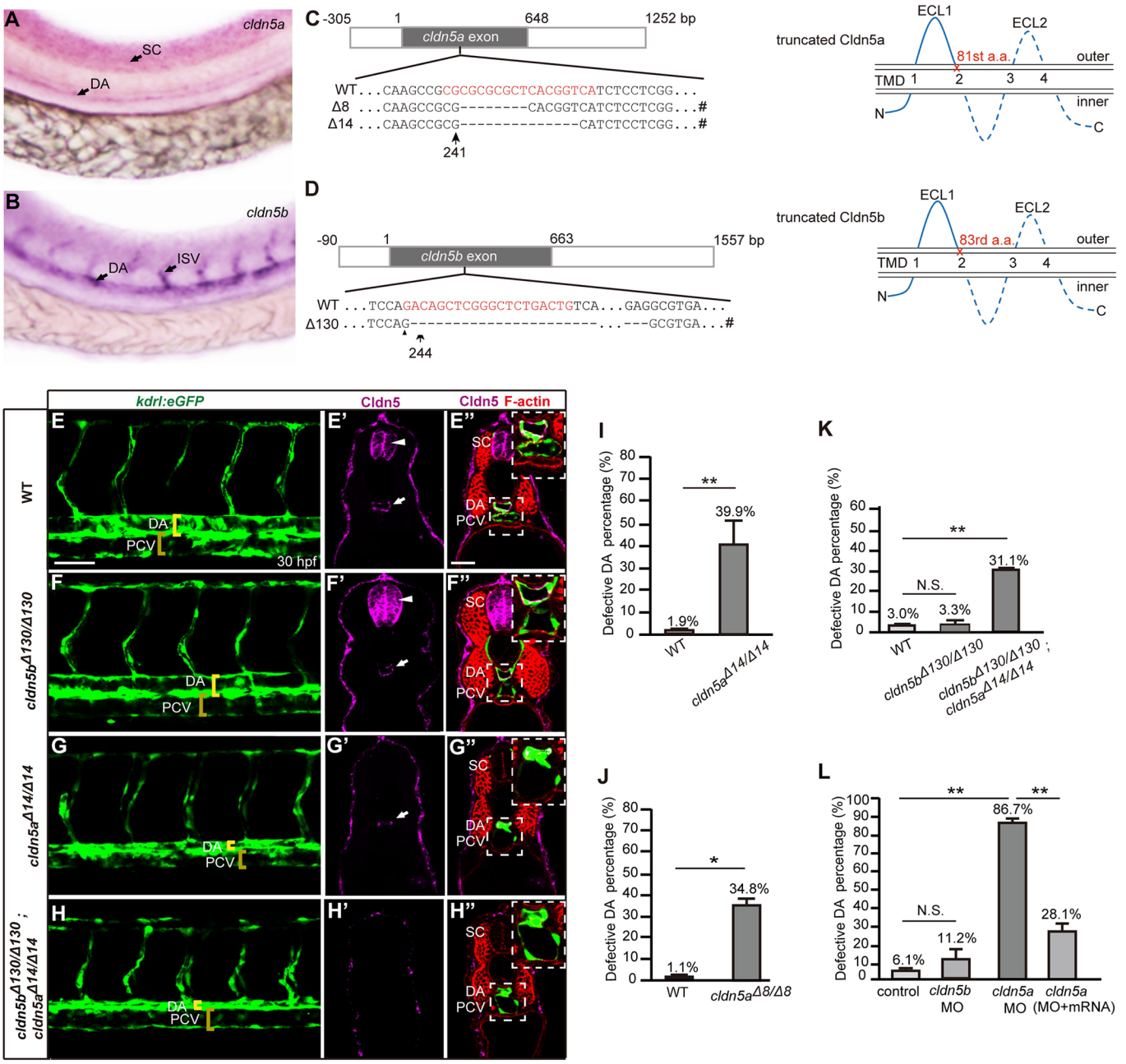

Fig. 3. See next page for legend.

controlling the selective adhesive forces required for the segregation of arterial versus venous endothelial progenitor cells. This effect may be mediated directly, via homophilic trans-interactions between opposing Cldn5 proteins, or by regulating the expression of other cell adhesion factors such as PECAM-1 and integrin-β1 (Fig. 6). In tune with such a model, loss of zebrafish Cldn5a resulted in increased motility and reduced cohesion of dorsal aorta progenitor ECs. Its loss also resulted in a failure of dorsal aorta to expand its lumen and to separate from caudal vein ECs. These findings suggest that Cldn5 may have dual functions. First, we suggest that it may provide the adhesive forces needed for limiting EC motility and for the developmental sorting of vascular progenitor cells. However, whether motility defects are directly caused by defects in cell adhesion remains to be clarified and will require additional experiments. Later, Cldn5 may contribute to the physiological adaptation of arterial ECs to their characteristic vessel permeability properties. Our findings are consistent with increasing evidence from *in vitro* cell studies reporting that claudins regulate adhesion, migration and proliferation of tumor cells (Escudero-Esparza et al., 2012; Kwon, 2013). The knockdown or overexpression of Cldn5 in hCMEC/D3 cells affects EC proliferation and migration, which causes a disruption of the blood–brain barrier permeability and an increased infiltration of tumor cells (Shmakov et al., 2017). Increased Cldn5 expression results in decreased cell motility and in reduced adhesion to the extracellular matrix (Escudero-Esparza et al., 2012). In sum, our study points at an adhesive role of Cldn5 during vasculogenesis of the zebrafish dorsal aorta. Intriguingly, this may be an evolutionarily conserved role related to non-canonical adhesive roles ascribed to claudin-related proteins that are essential for the assembly of the *Drosophila* heart tube (Yi et al., 2008).

Journal of Cell Science (2021) 134, jcs248237. doi:10.1242/jcs.248237

Fig. 3. Expression and developmental functions of zebrafish *claudin-5a* and *claudin-5b* during vasculogenesis. (A) Whole-mount *in situ* hybridizations showing that zebrafish *cldn5a* is expressed within the spinal cord (SC) and dorsal aorta (DA) at 30 hpf. (B) *cldn5b* is highly expressed in the DA and intersegmental vessels (ISVs). (C) Nucleotide sequence of the *cldn5a* target site. The two *cldn5a* alleles have an 8 bp (*cldn5a*$^{\Delta 8}$) and a 14 bp deletion (*cldn5a*$^{\Delta 14}$) after nucleotide position 241. Both mutations encode predicted truncations from amino acid (a.a.) 81 at the second transmembrane domain (TMD). (D) Nucleotide sequence of the *cldn5b* target site. The *cldn5b*$^{\Delta 130}$ mutant allele has a 130 bp nucleotide deletion after nucleotide position 244, which leads to a predicted Cldn5b truncation from a.a. 83 at the second TMD in *cldn5b*$^{\Delta 130/\Delta 130}$ mutant. Dashes indicate deletions. (E–H) Confocal *Z*-stack maximal projection images with lateral views of trunk region in endothelium-specific *Tg(kdrl:egfp)*^{s843} transgenic zebrafish embryos. Brackets indicate the diameter of the DA and posterior cardinal vein (PCV). In *cldn5a* mutant (G) and *cldn5a*;*cldn5b* double mutant (H), DAs are collapsed. (E′–H″) Shown are immunohistochemical stainings with an anti-pan Cldn5 antibody, which recognizes both Cldn5a and Cldn5b, on vibratome-sectioned trunk tissue of endothelium-specific *Tg(kdrl:egfp)*^{s843} transgenic zebrafish embryos. (E′,E″) In wild-type (WT), Cldn5 is expressed in both SC (arrowhead) and endothelial cells of the DA (arrow). (F′,F″) In *cldn5b*$^{\Delta 130/\Delta 130}$ mutants, Cldn5 protein is expressed in both SC (arrowhead) and DA (arrow). Loss of Cldn5b does not affect the formation of DA or PCV. (G′,G″) In *cldn5a*$^{\Delta 14/\Delta 14}$ mutants, Cldn5 protein is detected only in the DA (arrow) but not in the SC. Loss of Cldn5a causes a failure of the lumenization of the dorsal aorta. (H′,H″) In *cldn5a*$^{\Delta 14/\Delta 14}$; *cldn5b*$^{\Delta 130/\Delta 130}$ double mutants, Cldn5 immunoreactivity is lost in both SC and DA and the DA fails to expand during vasculogenesis, while the formation of the PCV is not affected. (I–L) Quantifications (means±s.e.m.) of percentages of embryos with a defective lumen expansion of the DA. (I) *cldn5a*$^{\Delta 14/\Delta 14}$ mutants (*n*=243 embryos) and cldn5a MO-injected *cldn5a*$^{\Delta 14/\Delta 14}$ mutants (*n*=283 embryos), (J) *cldn5a*$^{\Delta 8/\Delta 8}$ mutants (*n*=95 total embryos), and (K) *cldn5a*$^{\Delta 14/\Delta 14}$; cldn5b$^{\Delta 130/\Delta 130}$ double mutants (*n*=103 embryos) show an incomplete penetrance of the phenotype while *cldn5b*$^{\Delta 130/\Delta 130}$ mutants have the normal phenotype of DA and PCV (*n*=129 embryos). (L) In *cldn5a* but not *cldn5b* morphants the dorsal aorta expansion phenotype is highly penetrant (*n*=198 total embryos for *cldn5a* morphants and *n*=166 embryos for *cldn5b* morphants). The specificity of this phenotype was assessed by injecting exogenous *cldn5a* mRNA which rescued the dorsal aorta lumenization phenotype (*n*=299 embryos). Insets in E″–H″ are magnifications of the DA and PCV regions. DA, dorsal aorta; PCV, posterior cardinal vein; SC, spinal cord. **P*<0.05; ***P*<0.01; N.S., not significant (unpaired two-tailed Student's *t*-test). Scale bars: 75 µm (E); 20 µm (E″).

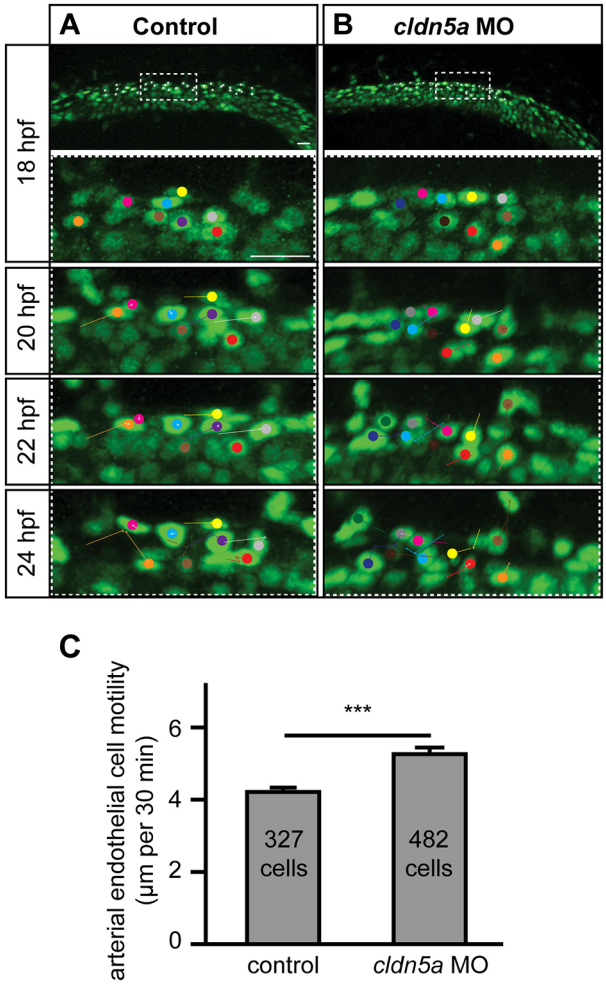

Fig. 4. Time-series based on confocal images of vasculogenesis of the dorsal aorta between 17 and 24 hpf. (A) Lateral overview from *Tg(fli1:nEGFP)*^{y7} control embryo (taken from Movie 5) or (B) *cldn5a* morphant embryo (taken from Movie 6). White dots indicate the tracked cells. Dashed rectangle indicates the area of the embryo shown with higher resolution at 18, 20, 22 and 24 hpf. Each cell is marked with a different color and followed over time. Lines in colors represent the increasing displacement of each cell from the first time point. (C) Quantification (means±s.d.) of the speed of arterial endothelial cells from a five-somite region of control embryos (*n*=6) or *cldn5a* morphant embryos (*n*=6) between 17 hpf to 24 hpf. ****P*<0.001 (unpaired two-tailed Student's *t*-test). Scale bars: 20 µm.

MATERIALS AND METHODS

Zebrafish handling and maintenance

Zebrafish transgenic lines *Tg(gata1:DsRed)* (Traver et al., 2003), *Tg(kdrl:eGFP)*^{s843} (Jin et al., 2005) and *Tg(fli1:nEGFP)*^{y7} (Siekmann and Lawson, 2007) were maintained according to standard laboratory procedures (Kimmel et al., 1995; Westerfield, 2007). Fertilized embryos were raised in 0.003% phenylthiourea (P7629, Sigma), which was added to the embryo medium at 24 hpf to inhibit pigment formation. Handling of zebrafish was performed in accordance with Guangdong State Regulations on Laboratory Animal Management, and German and Brandenburg state law, carefully monitored by the local authority for animal protection (LAVG, Brandenburg, Germany).

Generation of *cldn5a* and *cldn5b* mutants

CRISPR/Cas9 technology was utilized to generate *cldn5a* and *cldn5b* mutants. *Cas9* mRNA was synthesized using T7 mMESSAGE mMACHINE® Kit (AM1344, Ambion, USA) and guide RNA was *in vitro* transcribed following the T7 MAXIscript® Kit manual (AM1312, Ambion, USA). To generate stable *cldn5a* or *cldn5b* mutants, guide RNA (150 ng/µl) and *Cas9* mRNA (250 ng/µl) were co-injected into one-cell stage wild-type embryos. Founders and F1 generation animals were genotyped by DNA sequencing. Two *cldn5a* mutant alleles (*cldn5a*$^{\Delta 14}$ and *cldn5a*$^{\Delta 8}$) and one *cldn5b* mutant (*cldn5b*$^{\Delta 130}$) were identified via sequencing. Adult zebrafish were genotyped using PCR amplification products generated using specific primers (Table S1).

CRISPR/Cas13a-mediated *cldn5a* knockdown

In brief, *cas13a* from *Leptotrichia shahii* was cloned in *pCS2+* plasmid and the plasmid was linearized with *Xba*I. Then, *cas13a* mRNA was amplified using mMESSAGE mMACHINE®SP6 Transcription Kit (Roche) with the promoter of *SP6*. Zebrafish *cldn5a* crRNA (5′-GGTGGGGTTATAGCTT-CCCCTGATTTTGGAGCGCGACGACGCTCAAGACCGAGGAG-3′) was amplified using the mMESSAGE mMACHINE®T7 *in vitro* transcription kit. For injection into the one-cell stage embryos, the following concentration was used: *cas13a*, 1500 ng/µl and *cldn5a* crRNA, 500 ng/µl. Only *cldn5a* crRNA of 500 ng/µl was injected as control. For the analysis of the knockdown efficiency, qRT-PCR of *cldn5a* was performed with RNA extracted from different groups of embryos. Primers used for *cldn5a* crRNA amplification and qRT-PCR are listed in Table S1.

Whole-mount *in situ* hybridizations

Zebrafish *cldn5a* or *cldn5b* cDNAs were amplified from a standard cDNA library and were cloned into *pGEM-T* vector. To synthesize Dig-labeled antisense mRNA probes, recombinant plasmids were linearized with *NcoI* (R0193V, New England BioLabs, Ipswich, MA) and transcribed with *SP6* RNA polymerase using Dig RNA Labeling kit (11175025910, Roche, Switzerland). Whole-mount *in situ* hybridization (WISH) was performed as

Journal of Cell Science (2021) 134, jcs248237. doi:10.1242/jcs.248237

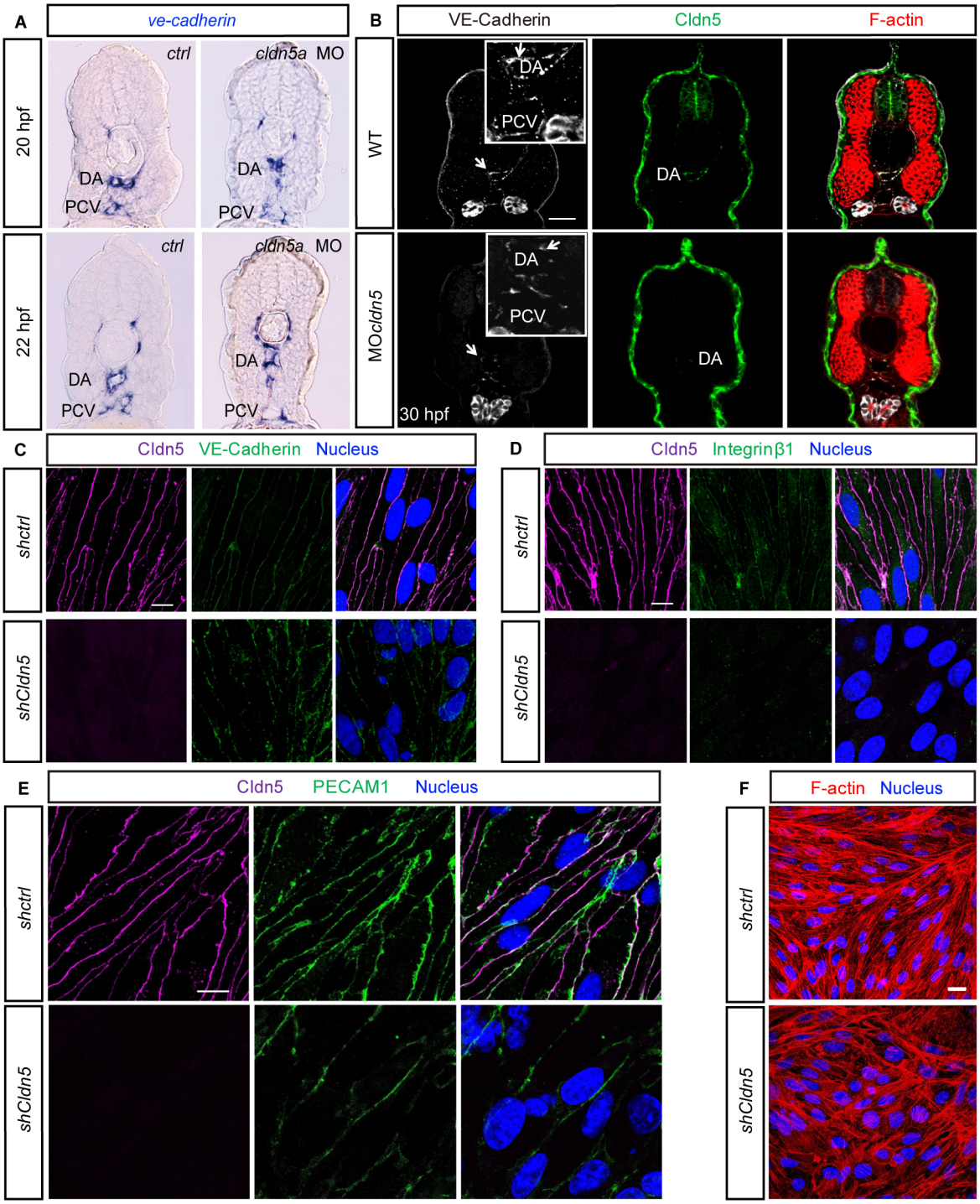

Fig. 5. Effects of Claudin-5 on the expression and localization of endothelial adhesive molecules. (A) Whole-mount *in situ* hybridizations of *ve-cadherin* expression in dorsal aortic and venous ECs showing that it is not affected upon loss of Cldn5a at 20 and 22 hpf, respectively. (B) Immunohistochemical stainings of cross sections through the embryonic trunk region showing that expression and localization of VE-Cadherin (white arrows) in dorsal aorta (DA) and posterior cardinal vein (PCV) is not affected upon loss of Cldn5a. Insets are magnifications of the DA and PCV regions. (C–E) The expression of PECAM1 (D) and integrin-β1 (E) but not VE-Cadherin (C) in bEnd.3 cells is affected by loss of Cldn5. (F) The cytoskeletal filamentous actin (F-actin) has a normal expression in *shCldn5*-bEnd.3 cells. DA, dorsal aorta; PCV, posterior cardinal vein. Scale bars: 75 µm (B); 10 µm (C–F).

previously described (Hauptmann and Gerster, 1994). Following WISH of *ve-cadherin*, whole embryos were incubated in 30% sucrose for 24 h at 4°C and then embedded within an optimum cutting temperature compound (4583, SAKURA), flash-frozen in liquid nitrogen, and cryosectioned into 10-µm-thickness sections, followed by 0.05% Neutral Red (N3246, Thermo Fisher, USA) staining for 12 s.

Vibratome sectioning and immunohistochemistry staining

Embryos were fixed with 4% PFA overnight at 4°C. Serial trans-sections of embryonic trunk vessel parts with a thickness of 150 µm were made using a VT1000S vibratome (Leica, Germany). Immunofluorescence stainings were performed as follows. Embryonic tissue sections were blocked for 60–100 min in PBS with 0.1% Tween 20 and 1% DMSO (PBDT) plus 5% (v/v) normal

Journal of Cell Science (2021) 134, jcs248237. doi:10.1242/jcs.248237

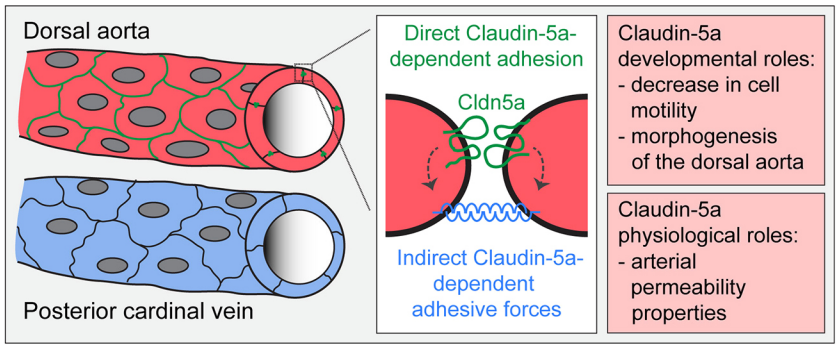

Fig. 6. Model on the roles of Claudin-5a during vasculogenesis of the zebrafish dorsal aorta. The expression of Cldn5a is restricted to endothelial cells of the dorsal aorta. Within this blood vessel, Cldn5a regulates paracellular barrier properties as a component of the tight junctions. During the development of the dorsal aorta, Cldn5a may generate adhesive forces via a direct mechanism involving homophilic *trans*-cellular interactions or by an indirect mechanism via regulating the expression of other cell adhesion factors (i.e. PECAM-1 and integrin-β1). Such mechanisms may limit endothelial cell motility.

goat serum (NGS) at room temperature (RT), then incubated with goat anti-mouse Cldn5 antibody (35-2500, Thermo Fisher Scientific; diluted 1:200 in PBDT, 5% NGS and 1% BSA) or anti-VE-Cadherin antibody (diluted 1:50 in PBDT, 5% NGS and 1% BSA) (Blum et al., 2008) overnight at 4°C. During the second day, sections were washed eight times for 10 min each time in PBDT, plus 1% NGS and 0.1 M NaCl (last wash in PBDT plus 1% NGS). Secondary antibodies conjugated with Alexa Fluor 647 (115-605-003, Jackson; diluted 1:200 in PBDT, 5% NGS and 1% BSA) and Rhodamine–phalloidin fluorescent dye (R415, Invitrogen, diluted 1:400 in PBDT+5% NGS+1% BSA) against F-actin were used to incubate embryonic tissue sections overnight at 4°C. After staining, sections were washed eight times for 10 min each time in PBDT plus 1% NGS and 0.1 M NaCl. Finally, slices were kept in the dark in PBS with 0.1% Tween 20 (PBST) (pH 7.4) at 4°C and mounted in anti-Slow Fade (S36936, Life Technologies) prior to imaging.

Antisense oligonucleotide morpholinos, mRNA synthesis and microinjection

Morpholino antisense oligonucleotides (MOs) were purchased from GeneTools, and dissolved to 1 mM stock solutions in RNase-free water. One-cell stage embryos were injected with 4 nl of 150 µM *cldn5a*-MO (Zhang et al., 2010) or 300 µM *cldn5b*-MO (Zhang, 2010) for single MO-mediated knockdowns, and 4 nl of 100 µM *cldn5a*-MO together with 200 µM *cldn5b*-MO for double MO-mediated knockdowns. MO sequences are listed in Table S1. For rescue experiments, full-length cDNA encoding Cldn5a was generated by PCR and fused to the 3′ terminus of an *egfp* cDNA fragment. The *egfp-cldn5a* was then cloned into *pCS2+* vector. The mMESSAGE mMACHINE Kit (AM1344, Ambion, USA) was used to synthesize capped mRNA. One-cell stage embryos were injected with 200 µM of *cldn5a*-MO or 200 µM *cldn5a*-MO together with 200 ng/µl *egfp-cldn5a* mRNA in a total volume of 4 nl.

Imaging

Embryos with immunohistochemical staining were mounted in anti-Slow Fade (S36936, Life Technologies, USA). WISH stainings of embryos were imaged on an Olympus BX51/DP71 microscope (TOKYO, JAPAN) and images of frozen sections of WISH-stained embryos were captured using an Olympus BX/DP80 microscope (TOKYO, JAPAN). All images of cells were acquired on a Leica M205FA stereo microscope (Leica, Germany).

In vivo time-lapse movies of live embryos

For time-lapse confocal microscopy imaging (as shown in Fig. 4) *Tg(fli1:nEGFP)*^{y7} zebrafish embryos were dechorionated at the 17-somite stage and mounted with a lateral orientation on a glass bottom dish in 0.8% low-melting agarose (16520-100, Thermo Fisher Scientific, USA), with E3 medium containing 0.4 mg/ml Tricaine (3-amino benzoic acidethylester, Sigma-Aldrich, A-5040), positioned within a chamber and maintained at 28°C. Images for each embryo were recorded every 30 min during a period of 7 h on a LSM 710 confocal microscope (Zeiss) with a 20× objective. For image processing, Imaris (Bitplane, Version 7.7) was used to perform semi-automatic cell tracking of dorsal aorta ECs. For statistical analysis, the track length of each EC cell within a 5-somite wide region was divided by its total track duration (with a threshold of 3 time points). The average trajectories for each ECs' displacement within 30 min were analyzed by an unpaired two-tailed Student's *t*-test with Microsoft Excel 2010.

Cell culture and immunolabeling

Murine brain microvascular endothelial cells (bEnd.3) obtained from Shanghai Bioleaf Biotech were maintained in Dulbecco's modified Eagle's medium (C11995500BT, Gibco, Thermo Fisher Scientific) supplemented with 10% FBS at 37°C in a 5% CO_2 incubator. A *Cldn5* knockdown cell line (*shcldn5*-bEnd.3 cell) was generated as described in our previous study (Liao et al., 2016). Human brain microvascular endothelial cells (HBMECs) were purchased from MingzhouBio (https://www.mingzhoubio.com/, cat. no. C-12287). The HBMEC *Cldn5*$^{-/-}$-mutated line was generated by CRISPR/Cas9 strategy using sgRNA (5′-CGACAGACCCGCGGGGCA-AA-3′). The bEnd.3 *Cldn5*$^{-/-}$ mutated line was generated by CRISPR/Cas9 strategy using sgRNA (5′-CCACAACATCGTGACGGCGCAGA-3′). The expression of endothelial Cldn5 was then analyzed by western blotting and immunolabeling with anti-Cldn5 antibody. For EC culturing, the culture medium was changed every 2 days and the cells were cultured for ∼5 days until formation of a monolayer was completed. For immunostainings, monolayers of bEnd.3 or HBMECs were cultured on beads or coverslips and were fixed with acetone for 10 min on ice. After blocking (1% BSA and 0.2% Tween-20 in PBS) for 1 h, fixed cells were then incubated with primary antibodies diluted 1:200 in blocking solution, overnight at 4°C. The following primary antibodies were used: pan-Cldn5 monoclonal antibody (Invitrogen, 35-2500), ZO-1 polyclonal antibody (Invitrogen, 40-2200), VE-cadherin polyclonal antibody (Santa Cruz Biotechnology, sc-28644), PECAM-1 (CD31) monoclonal antibody (eBioscience, 14-0311-81), integrin-β1 monoclonal antibody (Abcam, ab24693). For secondary antibody stainings, cells were subsequently incubated with Alexa Fluor 488-conjugated goat anti-mouse IgG (1:200; Jackson ImmunoResearch), Alexa Fluor 647-conjugated goat anti-rabbit IgG (1:200; Jackson ImmunoResearch), Rhodamine–phalloidin (1:500; Invitrogen) and DAPI (1:1000; Sigma-Aldrich) for 1 h at 37°C. Finally, stained cells were imaged using a Leica TCS SPII 5 confocal microscope (Leica, Solms, Germany).

Atomic force microscopy

The AFM assay was performed as previously reported (Chen et al., 2017a; Flach et al., 2011). In brief, bEnd.3 or *shcldn5* bEnd.3 cells were cultured on collagen-coated glass plates/slides or glass beads until a cell monolayer formed. The plates/slides were placed onto an AFM-compatible chamber. A clean cantilever coated with Cell-Tak (Corning CoStar Corporation, Cambridge, MA) was made to adhere to the cell-covered bead. During each cycle of measurements, the AFM cantilever carrying the cell-covered bead was incrementally lowered by 0.5–2 µm steps to make contact with the cells covering the basal plate/slide until the first force curve was generated. The cell on the cantilever interacted with the cell on the disk for 5 min before the cantilever was moved upwards to separate completely. This process was carried out in an incubated chamber with stable 37°C and 5% CO_2 conditions. Data from five independent sample tests was collected and normalized by using the JPK image processing software (Bruker/JPK NanoWizard, Berlin, Germany).

Bead rolling measurement

Bead rolling measurements were conducted as previously described (Strilić et al., 2010). Briefly, bEnd.3, bEnd.3 *Cldn5*$^{-/-}$ or *shcldn5*-bEnd.3 cells were cultured on six-well cell culture plates or collagen-coated glass beads until a cell monolayer formed. The cell culture plate was placed on a fixed

trestle with an inclination angle of 21° under a stereo-microscope (M205FA, Leica, Germany). The cell-covered bead then rolled upon the plate/slide containing the cell monolayer culture. Images of rolling beads were captured continuously every 30 s for a total duration of 5 min. The bead rolling distance was measured directly according to the start and end positions.

Cell migration assay

Cell migration assays were performed using modified 24-well TransWell inserts (pore size, 8 µm; diameter, 6.5 mm; Costar, Acton, MA) according to the manufacturer's instruction. Briefly, bEnd.3, bEnd.3 *Cldn5*$^{-/-}$ or *shcldn5*-bEnd.3 cells, with a density of 10^5 cells/well cultured in 200 µl 10% FBS medium, were seeded within the upper chamber, and 1.1 ml 10% FBS medium with or without endothelial cell growth factor (92590, Millipore) was added within the lower chamber. After a 24 h incubation, cells on the upper or bottom surface were fixed with methanol and stained with 0.1% Crystal Violet (C0775, Sigma) for quantifications of the migration rate using a stereo microscope (M205FA, Leica, Germany).

Wound healing assay

BEnd.3, HBMEC, *shcldn5*-bEnd.3 bEnd.3 *Cldn5*$^{-/-}$ and HBMEC-*Cldn5*$^{-/-}$ cells were seeded into six-well dishes independently and cultured until ∼90% confluency. A sterilized pipette tip was used to scratch wounding across the cell monolayer. Migration of cells was observed and imaged under the microscope at serials of time point. Three wells of each group were quantified for each experimental condition. Experiments were carried out at least three times per group.

Statistical analysis

All statistical analyses were performed using Student's *t*-test (for two groups) or one-way ANOVA (for three or more groups) with Prism 5 software (GraphPad Software). In detail, a two-tailed method was applied for unpaired Student's test for both *in vivo* and *in vitro* experiments. The diameter of vessels and all *in vitro* cellular data are shown as means±s.d. Means±s.e.m. were used for trunk region vessel phenotypic ratios. 95% confidence intervals of data analyses were acquired for *in vivo* and *in vitro* experiments.

Acknowledgements

We thank Dr Dong Liu (Nantong University, China) for providing the *pCS2-Cas13a* plasmid. Thanks also to P. Yu, B. Wuntke, A. Hubig for technical assistance and to Y. Zheng, M. Kneisler for fish husbandry. For discussions of the project and critical reading of the manuscript we are indebted to all members of the Zhang's and Seyfried's groups and Russ Hodge.

Competing interests

The authors declare no competing or financial interests.

Author contributions

Conceptualization: J.Z.; Methodology: Z.Y., F.F., S.W., W.X., Z.G., Y.L., J.Z.; Formal analysis: Z.Y., F.F., S.W., W.X., Y.L., S.A.-S., J.Z.; Investigation: Z.Y., F.F., S.W., W.X., Z.G., Y.L., J.Z.; Resources: A.S., M.A., H.-G.B., J.Z.; Data curation: Z.Y., F.F., W.X., Z.G., J.Z.; Writing - original draft: J.Z.; Writing - review & editing: S.A.-S., J.Z.; Visualization: F.F., S.W., Z.G.; Supervision: J.Z.; Project administration: J.Z.; Funding acquisition: S.A.-S., J.Z.

Funding

This work was supported by the National Key Research and Development Program of China (2018YFA0801200, 2018YFA0801000), the National Natural Science Foundation of China (31970777, 31771628, 31370824) and Guangdong Natural Science Fund for Distinguished Young Scholars (2017A030306024) to J.Z. S.A.-S. was supported by a Deutsche Forschungsgemeinschaft (DFG) network grant for SFB958 and projects SE2016/7-2, SE2016/10-1 and SE2016/13-1.

Supplementary information

Supplementary information available online at
https://jcs.biologists.org/lookup/doi/10.1242/jcs.248237.supplemental

References

Abudayyeh, O. O., Gootenberg, J. S., Essletzbichler, P., Han, S., Joung, J., Belanto, J. J., Verdine, V., Cox, D. B. T., Kellner, M. J., Regev, A. et al. (2017). RNA targeting with CRISPR-Cas13. *Nature* **550**, 280-284. doi:10.1038/nature24049

Blum, Y., Belting, H.-G., Ellertsdottir, E., Herwig, L., Lüders, F. and Affolter, M. (2008). Complex cell rearrangements during intersegmental vessel sprouting and vessel fusion in the zebrafish embryo. *Dev. Biol.* **316**, 312-322. doi:10.1016/j.ydbio.2008.01.038

Bujko, M., Kober, P., Mikula, M., Ligaj, M., Ostrowski, J. and Siedlecki, J. A. (2015). Expression changes of cell-cell adhesion-related genes in colorectal tumors. *Oncol. Lett.* **9**, 2463-2470. doi:10.3892/ol.2015.3107

Chen, J., Ganguly, A., Mucsi, A. D., Meng, J., Yan, J., Detampel, P., Munro, F., Zhang, Z., Wu, M., Hari, A. et al. (2017a). Strong adhesion by regulatory T cells induces dendritic cell cytoskeletal polarization and contact-dependent lethargy. *J. Exp. Med.* **214**, 327-338. doi:10.1084/jem.20160620

Chen, J., Luo, Y., Hui, H., Cai, T., Huang, H., Yang, F., Feng, J., Zhang, J. and Yan, X. (2017b). CD146 coordinates brain endothelial cell-pericyte communication for blood-brain barrier development. *Proc. Natl. Acad. Sci. USA* **114**, E7622-E7631. doi:10.1073/pnas.1710848114

De Pascalis, C. and Etienne-Manneville, S. (2017). Single and collective cell migration: the mechanics of adhesions. *Mol. Biol. Cell* **28**, 1833-1846. doi:10.1091/mbc.e17-03-0134

Escudero-Esparza, A., Jiang, W. G. and Martin, T. A. (2012). Claudin-5 is involved in breast cancer cell motility through the N-WASP and ROCK signalling pathways. *J. Exp. Clin. Cancer Res.* **31**, 43. doi:10.1186/1756-9966-31-43

Flach, T. L., Ng, G., Hari, A., Desrosiers, M. D., Zhang, P., Ward, S. M., Seamone, M. E., Vilaysane, A., Mucsi, A. D., Fong, Y. et al. (2011). Alum interaction with dendritic cell membrane lipids is essential for its adjuvanticity. *Nat. Med.* **17**, 479-487. doi:10.1038/nm.2306

Fleming, A., Diekmann, H. and Goldsmith, P. (2013). Functional characterisation of the maturation of the blood-brain barrier in larval zebrafish. *PLoS ONE* **8**, e77548. doi:10.1371/journal.pone.0077548

Gootenberg, J. S., Abudayyeh, O. O., Lee, J. W., Essletzbichler, P., Dy, A. J., Joung, J., Verdine, V., Donghia, N., Daringer, N. M., Freije, C. A. et al. (2017). Nucleic acid detection with CRISPR-Cas13a/C2c2. *Science* **356**, 438-442. doi:10.1126/science.aam9321

Hauptmann, G. and Gerster, T. (1994). Two-color whole-mount in situ hybridization to vertebrate and Drosophila embryos. *Trends Genet.* **10**, 266. doi:10.1016/0168-9525(90)90008-T

Jeong, J.-Y., Kwon, H.-B., Ahn, J.-C., Kang, D., Kwon, S.-H., Park, J. A. and Kim, K.-W. (2008). Functional and developmental analysis of the blood-brain barrier in zebrafish. *Brain Res. Bull.* **75**, 619-628. doi:10.1016/j.brainresbull.2007.10.043

Jin, S.-W., Beis, D., Mitchell, T., Chen, J. N. and Stainier, D. Y. (2005). Cellular and molecular analyses of vascular tube and lumen formation in zebrafish. *Development* **132**, 5199-5209. doi:10.1242/dev.02087

Justus, C. R., Leffler, N., Ruiz-Echevarria, M. and Yang, L. V. (2014). In vitro cell migration and invasion assays. *J. Vis. Exp.* **88**, 51046, doi:10.3791/51046

Kim, J.-G., Bae, S.-J., Lee, H. S., Park, J.-H. and Kim, K.-W. (2017). Claudin5a is required for proper inflation of Kupffer's vesicle lumen and organ laterality. *PLoS ONE* **12**, e0182047. doi:10.1371/journal.pone.0182047

Kimmel, C. B., Ballard, W. W., Kimmel, S. R., Ullmann, B. and Schilling, T. F. (1995). Stages of embryonic development of the zebrafish. *Dev. Dyn.* **203**, 253-310. doi:10.1002/aja.1002030302

Kollmar, R., Nakamura, S. K., Kappler, J. A. and Hudspeth, A. J. (2001). Expression and phylogeny of claudins in vertebrate primordia. *Proc. Natl. Acad. Sci. USA* **98**, 10196-10201. doi:10.1073/pnas.171325898

Krause, G., Winkler, L., Mueller, S. L., Haseloff, R. F., Piontek, J. and Blasig, I. E. (2008). Structure and function of claudins. *Biochim. Biophys. Acta (BBA)-Biomembr.* **1778**, 631-645. doi:10.1016/j.bbamem.2007.10.018

Kubota, K., Furuse, M., Sasaki, H., Sonoda, N., Fujita, K., Nagafuchi, A. and Tsukita, S. (1999). Ca^{2+}-independent cell-adhesion activity of claudins, a family of integral membrane proteins localized at tight junctions. *Curr. Biol.* **9**, 1035-1038. doi:10.1016/S0960-9822(99)80452-7

Kwon, M. J. (2013). Emerging roles of claudins in human cancer. *Int. J. Mol. Sci.* **14**, 18148-18180. doi:10.3390/ijms140918148

Lal-Nag, M. and Morin, P. J. (2009). The claudins. *Genome Biol.* **10**, 235. doi:10.1186/gb-2009-10-8-235

Liao, Z., Yang, Z., Piontek, A., Eichner, M., Krause, G., Li, L., Piontek, J. and Zhang, J. (2016). Specific binding of a mutated fragment of Clostridium perfringens enterotoxin to endothelial claudin-5 and its modulation of cerebral vascular permeability. *Neuroscience* **327**, 53-63. doi:10.1016/j.neuroscience.2016.04.013

Liu, L., Li, X., Ma, J., Li, Z., You, L., Wang, J., Wang, M., Zhang, X. and Wang, Y. (2017). The Molecular architecture for RNA-guided RNA cleavage by Cas13a. *Cell* **170**, 714-726.e10. doi:10.1016/j.cell.2017.06.050

Loh, Y. H., Christoffels, A., Brenner, S., Hunziker, W. and Venkatesh, B. (2004). Extensive expansion of the claudin gene family in the teleost fish, fugu rubripes. *Genome Res.* **14**, 1248. doi:10.1101/gr.2400004

Ma, S.-C., Li, Q., Peng, J.-Y., Zhouwen, J.-L., Diao, J.-F., Niu, J.-X., Wang, X., Guan, X.-D., Jia, W. and Jiang, W.-G. (2017). Claudin-5 regulates blood-brain barrier permeability by modifying brain microvascular endothelial cell proliferation, migration, and adhesion to prevent lung cancer metastasis. *CNS Neurosci. Ther.* **23**, 947-960. doi:10.1111/cns.12764

Nitta, T., Hata, M., Gotoh, S., Seo, Y., Sasaki, H., Hashimoto, N., Furuse, M. and Tsukita, S. (2003). Size-selective loosening of the blood-brain barrier in claudin-5-deficient mice. *J. Cell Biol.* **161**, 653-660. doi:10.1083/jcb.200302070

Otani, T., Nguyen, T. P., Tokuda, S., Sugihara, K., Sugawara, T., Furuse, K., Miura, T., Ebnet, K. and Furuse, M. (2019). Claudins and JAM-A coordinately regulate tight junction formation and epithelial polarity. *J. Cell Biol.* **218**, 3372-3396. doi:10.1083/jcb.201812157

Piorntek, J., Winkler, L., Wolburg, H., Müller, S. L., Zuleger, N., Piehl, C., Wiesner, B., Krause, G. and Blasig, I. E. (2008). Formation of tight junction: determinants of homophilic interaction between classic claudins. *FASEB J.* **22**, 146-158. doi:10.1096/fj.07-8319com

Puech, P.-H., Taubenberger, A., Ulrich, F., Krieg, M., Muller, D. J. and Heisenberg, C. P. (2005). Measuring cell adhesion forces of primary gastrulating cells from zebrafish using atomic force microscopy. *J. Cell Sci.* **118**, 4199-4206. doi:10.1242/jcs.02547

Schneeberger, E. E. (1982). Structure of intercellular junctions in different segments of the intrapulmonary vasculature. *Ann. N. Y. Acad. Sci.* **384**, 54-63. doi:10.1111/j.1749-6632.1982.tb21361.x

Shmakov, S., Smargon, A., Scott, D., Cox, D., Pyzocha, N., Yan, W., Abudayyeh, O. O., Gootenberg, J. S., Makarova, K. S., Wolf, Y. I. et al. (2017). Diversity and evolution of class 2 CRISPR-Cas systems. *Nat. Rev. Microbiol.* **15**, 169-182. doi:10.1038/nrmicro.2016.184

Siekmann, A. F. and Lawson, N. D. (2007). Notch signalling limits angiogenic cell behaviour in developing zebrafish arteries. *Nature* **445**, 781-784. doi:10.1038/nature05577

Steinberg, M. S. (2007). Differential adhesion in morphogenesis: a modern view. *Curr. Opin. Genet. Dev.* **17**, 281-286. doi:10.1016/j.gde.2007.05.002

Strilić, B., Eglinger, J., Krieg, M., Zeeb, M., Axnick, J., Babál, P., Müller, D. J. and Lammert, E. (2010). Electrostatic cell-surface repulsion initiates lumen formation in developing blood vessels. *Curr. Biol.* **20**, 2003-2009. doi:10.1016/j.cub.2010.09.061

Traver, D., Paw, B. H., Poss, K. D., Penberthy, W. T., Lin, S. and Zon, L. I. (2003). Transplantation and in vivo imaging of multilineage engraftment in zebrafish bloodless mutants. *Nat. Immunol.* **4**, 1238-1246. doi:10.1038/ni1007

van Leeuwen, L. M., Evans, R. J., Jim, K. K., Verboom, T., Fang, X., Bojarczuk, A., Malicki, J., Johnston, S. A. and van der Sar, A. M. (2018). A transgenic zebrafish model for the in vivo study of the blood and choroid plexus brain barriers using claudin 5. *Biol. Open* **7**, bio030494. doi:10.1242/bio.030494

Westerfield, M. (2007). *The zebrafish Book: A Guide for the Laboratory use of Zebrafish (Danio Rerio)*, 5th edn. Eugene: University of Oregon Press.

Xie, J., Farage, E., Sugimoto, M. and Anand-Apte, B. (2010). A novel transgenic zebrafish model for blood-brain and blood-retinal barrier development. *BMC Dev. Biol.* **10**, 76. doi:10.1186/1471-213X-10-76

Yi, P., Johnson, A. N., Han, Z., Wu, J. and Olson, E. N. (2008). Heterotrimeric G proteins regulate a noncanonical function of septate junction proteins to maintain cardiac integrity in *Drosophila*. *Dev. Cell* **15**, 704-713. doi:10.1016/j.devcel.2008.10.001

Yu, J. A., Castranova, D., Pham, V. N. and Weinstein, B. M. (2015). Single-cell analysis of endothelial morphogenesis in vivo. *Development* **142**, 2951-2961. doi:10.1242/dev.123174

Zhang, J. (2010). *Investigation on Developmental Roles of the two Zebrafish Claudin5 Family Members*, 1st edn. CUVILLIER VERLAG Göttingen.

Zhang, J., Piontek, J., Wolburg, H., Piehl, C., Liss, M., Otten, C., Christ, A., Willnow, T. E., Blasig, I. E. and Abdelilah-Seyfried, S. (2010). Establishment of a neuroepithelial barrier by Claudin5a is essential for zebrafish brain ventricular lumen expansion. *Proc. Natl. Acad. Sci. USA* **107**, 1425-1430. doi:10.1073/pnas.0911996107

Zhang, J., Liss, M., Wolburg, H., Blasig, I. E. and Abdelilah-Seyfried, S. (2012). Involvement of claudins in zebrafish brain ventricle morphogenesis. *Ann. N. Y. Acad. Sci.* **1257**, 193-198. doi:10.1111/j.1749-6632.2012.06507.x

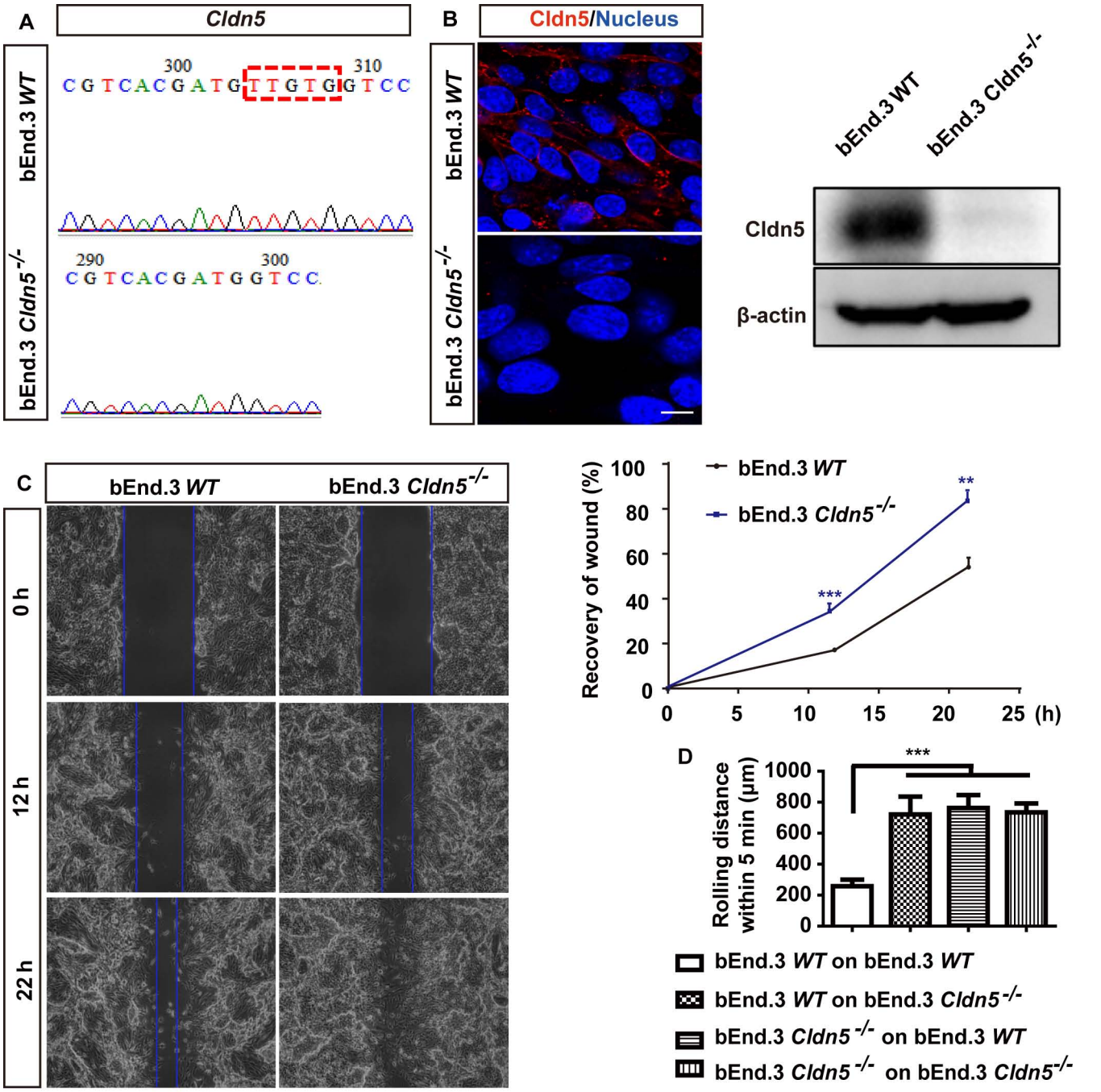

Supplementary Figure 1

Fig. S1. Knockout of *Claudin-5* in bEnd.3 cells increases cell motility. (A) CRIPSR/ Cas9-mediated gene editing induces a 5 bp nucleotide deletion of *Cldn5*. (B) Immunofluorescence staining and Western blot analyses of *Cldn5* knockout in bEnd.3 cells. (C) Representative images of wound healing assays with wild type or bEnd.3 *Cldn5*$^{-/-}$ cells. Images were taken at 0, 12 and 22 h respectively after the cell layer was scratched with a pipette tip. Statistical analyses of the wound recovery rate indicate a significantly increased migration ability of bEnd.3 *Cldn5*$^{-/-}$ cells after loss of Cldn5 compared with that of the wild type cells. n=3 tests per group. (D) Quantifications of the "rolling bead" assay with bEnd.3 and bEnd.3 *Cldn5*$^{-/-}$ cells. Knockout of *Cldn5* in bEnd.3 cells on either the culture plate or on the rolling bead reduces adhesion forces between endothelial cells. This correlates with a longer rolling distance of conditions with bEnd.3 *Cldn5*$^{-/-}$ cells-coated beads on bEnd.3 *Cldn5*$^{-/-}$ cells-coated culture plates compared with that of wild type bEnd.3-coated beads on wild type bEnd.3-coated culture plates. n=5 tests per group. **P<0.01, ***P<0.001; scale bar: 10 µm.

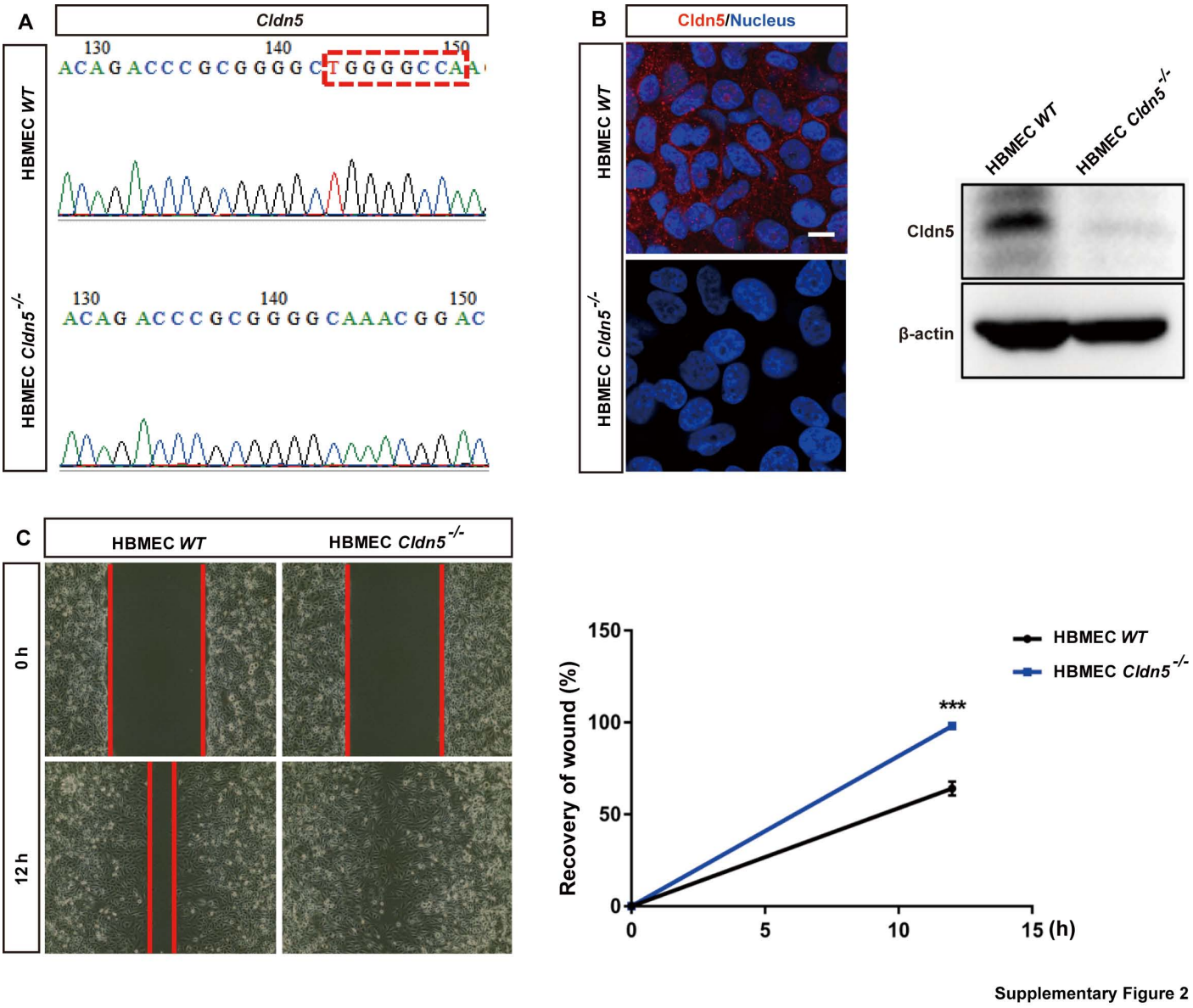

Fig. S2. Loss of *Claudin-5* in HBMECs increases cell motility. (A) CRIPSR/Cas9-mediated gene editing induces an 8 bp nucleotide deletion of *Cldn5*. (B) Immunofluorescence staining and Western blot analyses of *Cldn5* knockout in HBMEC cells. (C) Representative images of wound healing assays with wild type or HBMEC *Cldn5*$^{-/-}$ cells. Images were taken at 0, 12 h respectively after the cell layer was scratched with a pipette tip. Statistical analyses of the wound recovery rate indicate a significantly increased migration ability of HBMEC *Cldn5*$^{-/-}$ cells after loss of Cldn5 compared with that of the wild type cells. n=3 tests per group; ***P<0.001; scale bar: 10 µm.

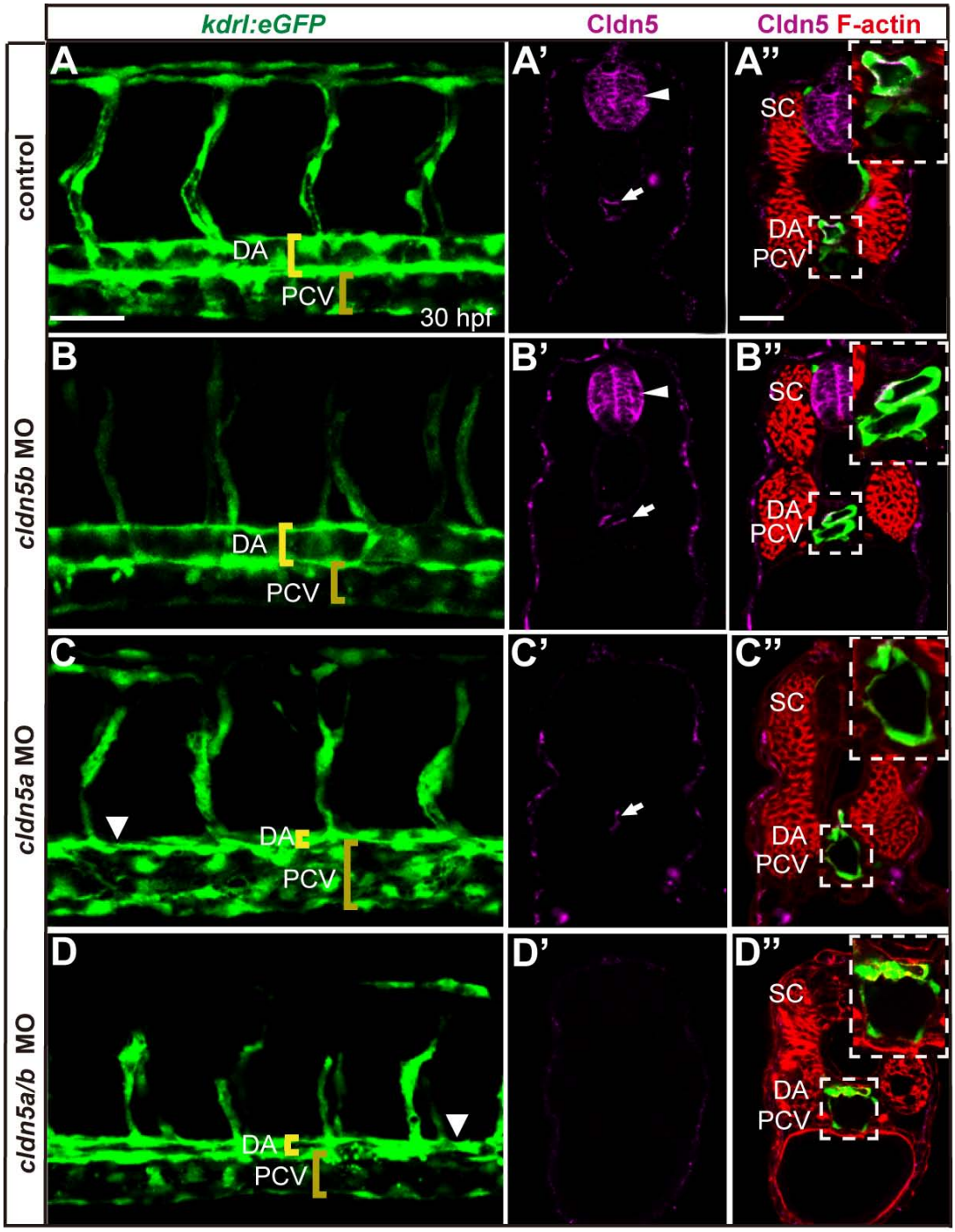

Supplementary Figure 3

Fig. S3. Expression of Claudin-5 proteins and vascular phenotypes in *claudin5a* and *claudin5b* morphants. (A-D) Confocal z-stack maximal projection images with lateral views of trunk region in endothelium-specific *Tg(kdrl:egfp)*^{s843}

transgenic zebrafish embryos. Indicated is the diameter of the dorsal aorta (DA) and posterior cardinal vein (PCV) (brackets). (C) Note the collapsed diameter in *cldn5a* morphants and (D) in *cldn5a*;*cldn5b* double morphants. (A'-D") Shown are immunohistochemical stainings with an anti-pan Cldn5 antibody which recognizes both Cldn5a and Cldn5b on vibratome-sectioned tissue of endothelium-specific *Tg(kdrl:egfp)*^{s843} reporter transgenic zebrafish embryos through the trunk region. (A', A") In wild-type, Cldn5 is expressed in both spinal cord (SC) (arrowhead) and in endothelial cells of the dorsal aorta (DA) (arrow). (B', B") In *cldn5b* morphants, Cldn5 protein is expressed in both SC (arrowhead) and DA (arrow). Loss of Cldn5b does not affect the formation of DA or posterior caudal vein (PCV). (C', C") In *cldn5a* morphants, Cldn5 protein is detected only in the DA (arrow) but not in the SC. Loss of Cldn5a causes a failure of the DA lumenization. (D', D") In *cldn5a*;*cldn5b* double morphants, Cldn5 immunoreactivity is lost in both SC and DA, and the DA fails to expand during vasculogenesis, while the formation of the PCV is not affected (n=199 total embryos). In severely defective regions along the vascular tube, DA and PCV are fused into one vascular tube (white triangles in C and D). Insets in A"-A" are high magnification scans of the DA and PCV regions. Scale bars: A, 75 µm; A", 20 µm.

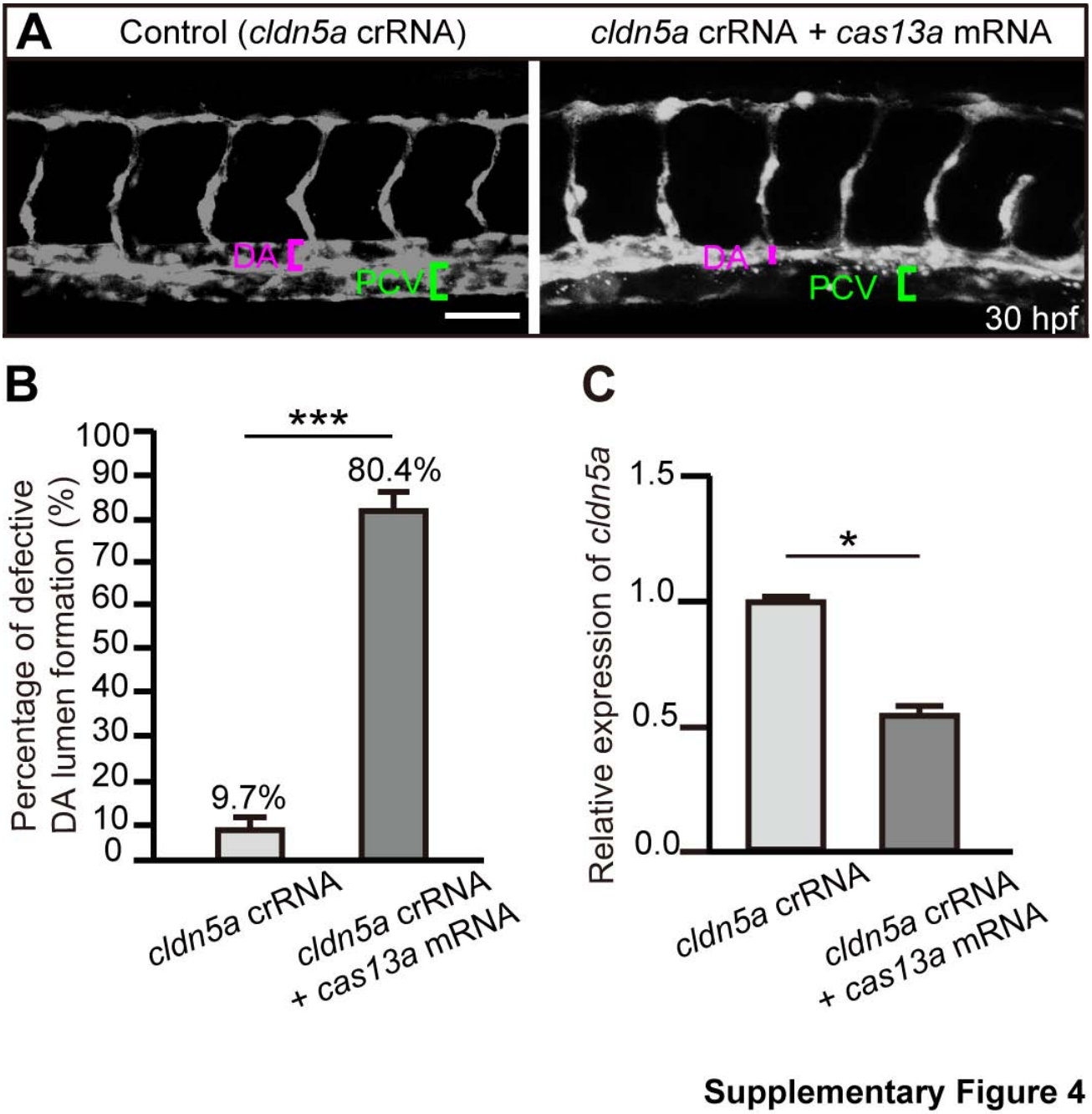

Supplementary Figure 4

Fig. S4. Efficient knockdown of zebrafish *claudin-5a* by CRISPR/Cas13a-mediated gene knockdown strategy and expression pattern of *ve-cadherin* after loss of *claudin-5a*. (A-B) Confocal z-stack maximal projection images with lateral views of trunk region in endothelium-specific *Tg(kdrl:egfp)*^{s843} transgenic zebrafish embryos at 30 hpf. Indicated is the diameter of the dorsal aorta (DA) and posterior cardinal vein (PCV) (brackets). (A) *cldn5a* crRNA-injected embryos were used as controls. (B) Quantification of percentages of embryos with a defective lumen expansion of the DA (n=257 embryos). (C) Quantitative reverse transcriptional-PCR (qRT-PCR) analyses of *cldn5a* mRNA expression upon CRISPR/Cas13a-mediated knockdown. *P<0.05, ***P<0.001; scale bar: 75 µm.

Movie 1. Bead rolling assay to reflect the cell adhesion force determined by Claudin-5. Representative time-lapse movie of bEnd.3-coated bead rolling on a tilted (inclination of 21°) bEnd.3 monolayer. Images were acquired every 12 s over a total time of 5 min. Related to Fig. 2.

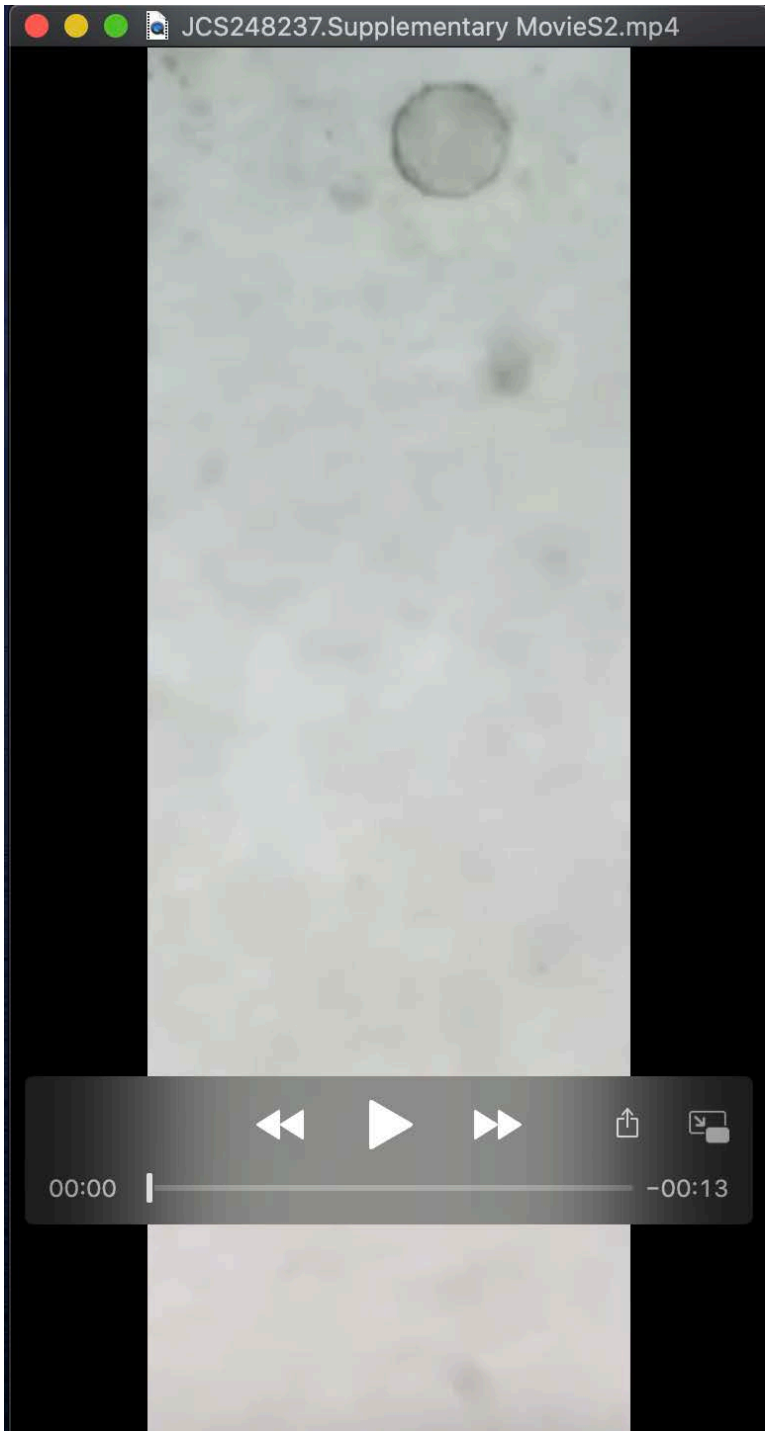

Movie 2. Bead rolling assay to reflect the cell adhesion force determined by Claudin-5. Representative time-lapse movie of bEnd.3-coated bead rolling on a tilted (inclination of 21°)*shCldn5*-bEnd.3 monolayer. Images were acquired every 12 s over a total time of 5 min. Related to Fig. 2.

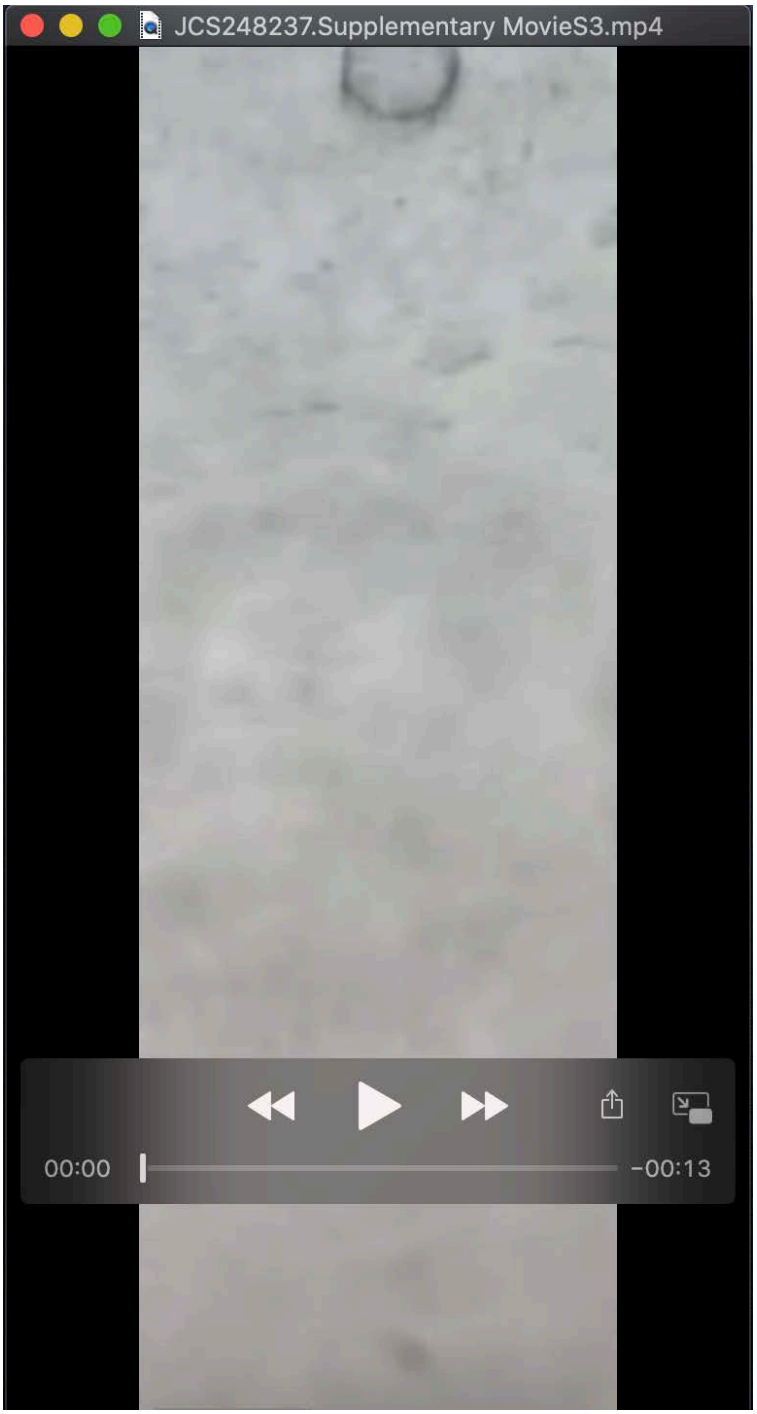

Movie 3. Bead rolling assay to reflect the cell adhesion force determined by Claudin-5. Representative time-lapse movie of *shCldn5*-bEnd.3-coated bead rolling on a tilted (inclination of 21°) bEnd.3 monolayer. Images were acquired every 12 s over a total time of 5 min. Related to Fig. 2.

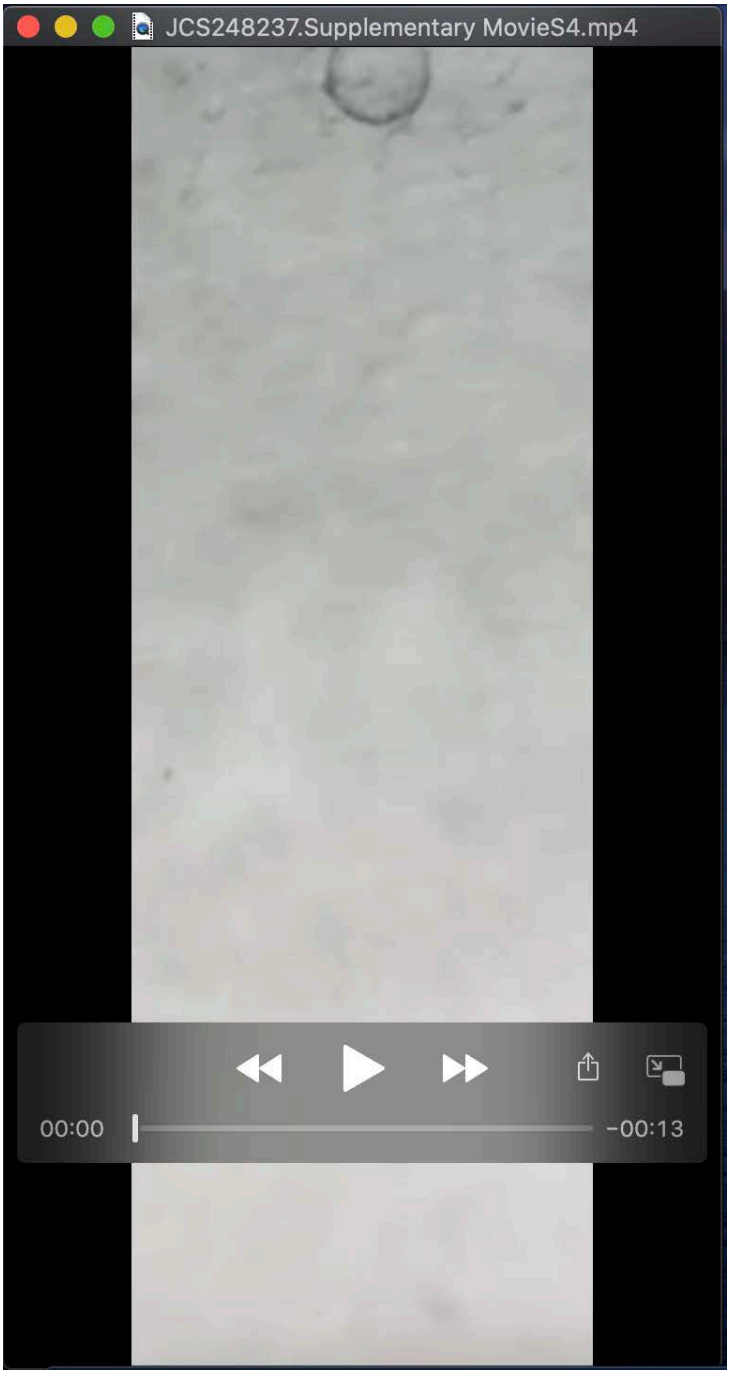

Movie 4. Bead rolling assay to reflect the cell adhesion force determined by Claudin-5. Representative time-lapse movie of *shCldn5*-bEnd.3-coated bead rolling on a tilted (inclination of 21°) *shCldn5*-bEnd.3 monolayer. Images were acquired every 12 s over a total time of 5 min. Related to Fig. 2.

Movie 5. Representative time-lapse movie of arterial endothelial cell migrations during vasculogenesis of the dorsal aorta. Shown is the endothelial-specific line *Tg(fli1:nEGFP)*^{y7}. White dots indicate single arterial endothelial cells. Images were acquired every 30 min over a total time of 7 h from 17 to 24 hpf. Scale bar: 30 µm. Related to Fig. 4A.

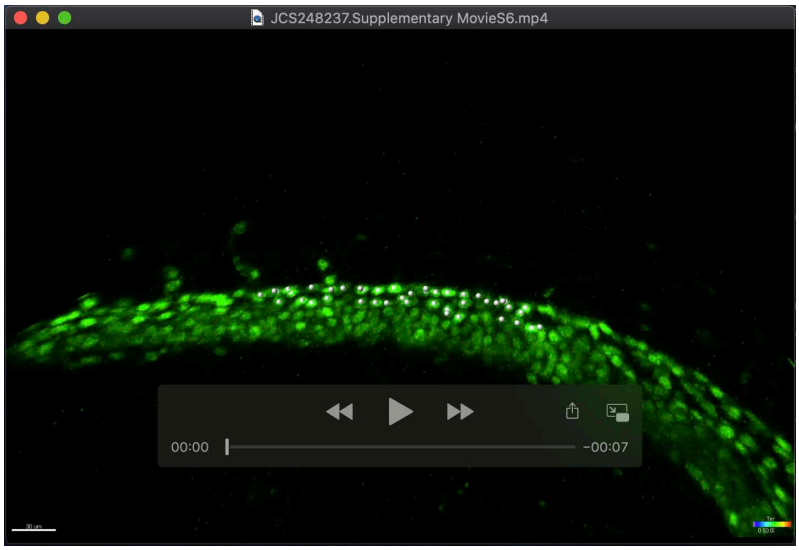

Movie 6. Representative time-lapse movie of arterial endothelial cell migrations during vasculogenesis of the dorsal aorta after knockdown of *claudin-5a*. Shown is the endothelial-specific line *Tg(fli1:nEGFP)*^{y7}. White dots indicate single arterial endothelial cells. Images were acquired every 30 min over a total time of 7 h from 17 hpf to 24 hpf. Scale bar: 30 µm. Related to Fig. 4B.

Table S1. Primers and morpholino sequences

Primers for genotyping	sequences
cldn5a mutant (for 14 nts deletion)	wild type Forward: 5′-GACCTGCAAGCCGCGCGCG-3′
	mutant Forward : 5′-GACCTGCAAGCCGCGCATCTC-3′
	universal Reverse : 5′-CGAGCAGCAGCAGCGCAGAGG-3′
cldn5a mutant (for 8 nts deletion)	wild type Forward : 5′-AAGCCGCGCGCGCGCT-3′
	mutant Forward : 5′-AAGCCGCGCACGGTCA-3′
	universal Reverse : 5′-CGAGCAGCAGCAGCGCAG-3′
cldn5b mutant	Forward : 5′-GTTGCCCATGTGGAAAGTGT-3′
	Reverse : 5′-CATCCAGCACAGAGGAATCA-3′
Primers for cDNA amplification	
cldn5a	Forward: 5′-ATGGCCTCCGCGGCTTTG-3′
	Reverse: 5′-ACACACACTCAAGCATTCACACGTA-3′
cldn5b	Forward: 5′-ATGGCAAATATGATTTCTGCATG-3′
	Reverse: 5′-TCAGACGTAGTTTCGTTTATCATAG-3′
ve-cadherin	Forward: 5′-TTCATGGTTGCTGTCCTGCTCACAT-3′
	Reverse: 5′-GCTCCCATTGGTTAGTTCTGGTGCAT-3′
Primers for *cldn5a* crRNA amplification	
cldn5a	Forward: 5′-TAATACGACTCACTATAGGGGGTGGGGTTATAGCT
	TCCCCTGATTTTGGAGCGCGACGACGCTCAAGACCGAGGAG-3'
	Reverse: 5'-CTCCTCGGTCTTGAGCGTCGTCGCGCTCCAAAATCA
	GGGGAAGCTATAACCCCACCCCCTATAGTGAGTCGTATTA-3'
Morpholinos	
cldn5a-MO	5′-AGGCCATCGCTTTCTTTTCCCACTC-3′
cldn5b-MO	5′-TCAGAAGCAGCAGAAGTGTCTCTAC-3′
Primers for qPCR	
cldn5a	Forward: 5′-GCCCACTAAAAGAGCCACAT-3′
	Reverse: 5′-AGAGTCCAGCGAAAAGCATC-3′
β-actin	Forward: 5'-GCTGCCTCTTCTTCCTCC-3'
	Reverse: 5'-ATGTCCACGTCGCACTTC-3'